Article

Neuron

Mutations in Chromatin Modifier and Ephrin Signaling Genes in Vein of Galen Malformation

Highlights

- Exome sequencing identifies genetic drivers of vein of Galen malformations (VOGMs)
- Mutations in chromatin modifier and Ephrin genes account for ~30% of VOGM cases
- Probands often exhibit vasculo-cutaneous lesions, suggesting a two-hit mechanism
- These data implicate impaired arterio-venous specification in VOGM pathogenesis

Authors

Daniel Duran, Xue Zeng, Sheng Chih Jin, ..., Murat Gunel, Richard P. Lifton, Kristopher T. Kahle

Correspondence

kristopher.kahle@yale.edu

In Brief

Vein of Galen malformations (VOGMs) are the most severe neonatal brain arterio-venous malformations. Duran et al. identify *de novo* chromatin modifier and rare inherited Ephrin signaling mutations in ~30% of VOGM cases. The data implicate disrupted arterio-venous specification in VOGM pathogenesis.

Duran et al., 2019, Neuron *101*, 1–15
February 6, 2019 © 2018 Elsevier Inc.
https://doi.org/10.1016/j.neuron.2018.11.041

CellPress

Please cite this article in press as: Duran et al., Mutations in Chromatin Modifier and Ephrin Signaling Genes in Vein of Galen Malformation, Neuron (2018), https://doi.org/10.1016/j.neuron.2018.11.041

Neuron
Article

Mutations in Chromatin Modifier and Ephrin Signaling Genes in Vein of Galen Malformation

Daniel Duran,[1,24] Xue Zeng,[2,24] Sheng Chih Jin,[2,3,24] Jungmin Choi,[2,3,24] Carol Nelson-Williams,[2] Bogdan Yatsula,[4] Jonathan Gaillard,[1] Charuta Gavankar Furey,[1] Qiongshi Lu,[5] Andrew T. Timberlake,[2] Weilai Dong,[2] Michelle A. Sorscher,[6] Erin Loring,[2] Jennifer Klein,[7] August Allocco,[1] Ava Hunt,[1] Sierra Conine,[1] Jason K. Karimy,[1] Mark W. Youngblood,[1,2] Jinwei Zhang,[8] Michael L. DiLuna,[1] Charles C. Matouk,[1] Shrikant Mane,[9] Irina R. Tikhonova,[9] Christopher Castaldi,[9] Francesc López-Giráldez,[9] James Knight,[9] Shozeb Haider,[10] Mariya Soban,[10,11] Seth L. Alper,[12] Masaki Komiyama,[13] Andrew F. Ducruet,[14] Joseph M. Zabramski,[14] Alan Dardik,[4] Brian P. Walcott,[15] Christopher J. Stapleton,[16] Beverly Aagaard-Kienitz,[17] Georges Rodesch,[18] Eric Jackson,[19] Edward R. Smith,[20] Darren B. Orbach,[7,20] Alejandro Berenstein,[6] Kaya Bilguvar,[2,9] Miikka Vikkula,[21] Murat Gunel,[1,2] Richard P. Lifton,[2,3,25] and Kristopher T. Kahle[1,22,23,25,26,*]

[1]Department of Neurosurgery, Yale School of Medicine, New Haven, CT, USA
[2]Department of Genetics, Yale School of Medicine, New Haven, CT, USA
[3]Laboratory of Human Genetics and Genomics, The Rockefeller University, New York, NY, USA
[4]Department of Surgery, Yale School of Medicine, New Haven, CT, USA
[5]Department of Biostatistics and Medical Informatics, University of Wisconsin-Madison, Madison, WI, USA
[6]Department of Neurosurgery, Icahn School of Medicine at Mount Sinai, New York, NY, USA
[7]Department of Neurosurgery, Boston Children's Hospital, Boston, MA, USA
[8]Institute of Biomedical and Clinical Sciences, University of Exeter Medical School, Hatherly Laboratory, Exeter, UK
[9]Yale Center for Genome Analysis, West Haven, CT, USA
[10]University College London, School of Pharmacy, London, UK
[11]Department of Biochemistry, Aligarh Muslim University, Aligarh, India
[12]Division of Nephrology and Center for Vascular Biology Research, Beth Israel Deaconess Medical Center, and Department of Medicine, Harvard Medical School, Boston, MA, USA
[13]Department of Neurointervention, Osaka City General Hospital, Osaka, Japan
[14]Department of Neurosurgery, Barrow Neurological Institute, Phoenix, AZ, USA
[15]Department of Neurological Surgery, University of Southern California, Los Angeles, CA, USA
[16]Department of Neurological Surgery, Massachusetts General Hospital and Harvard Medical School, Boston, MA, USA
[17]Department of Neurological Surgery, University of Wisconsin, Madison, WI, USA
[18]Service de Neuroradiologie Diagnostique et Thérapeutique, Hôpital Foch, Suresnes, France
[19]Department of Neurosurgery, Johns Hopkins University School of Medicine, Baltimore, MD, USA
[20]Department of Neurointerventional Radiology, Boston Children's Hospital, Boston, MA, USA
[21]Human Molecular Genetics, de Duve Institute, Université Catholique de Louvain, Brussels, Belgium
[22]Department of Pediatrics, Yale School of Medicine, New Haven, CT, USA
[23]Department of Cellular and Molecular Physiology, Yale School of Medicine, New Haven, CT, USA
[24]These authors contributed equally
[25]Senior author
[26]Lead Contact
*Correspondence: kristopher.kahle@yale.edu
https://doi.org/10.1016/j.neuron.2018.11.041

SUMMARY

Normal vascular development includes the formation and specification of arteries, veins, and intervening capillaries. Vein of Galen malformations (VOGMs) are among the most common and severe neonatal brain arterio-venous malformations, shunting arterial blood into the brain's deep venous system through aberrant direct connections. Exome sequencing of 55 VOGM probands, including 52 parent-offspring trios, revealed enrichment of rare damaging *de novo* mutations in chromatin modifier genes that play essential roles in brain and vascular development. Other VOGM probands harbored rare inherited damaging mutations in Ephrin signaling genes, including a genome-wide significant mutation burden in *EPHB4*. Inherited mutations showed incomplete penetrance and variable expressivity, with mutation carriers often exhibiting cutaneous vascular abnormalities, suggesting a two-hit mechanism. The identified mutations collectively account for ~30% of studied VOGM cases. These findings provide insight into disease biology and may have clinical implications for risk assessment.

INTRODUCTION

Embryogenesis requires vascular development to meet hemodynamic and nutritive demands. Arterio-venous (A-V) specification in model organisms is genetically determined and results in differential expression of genes in arteries and veins prior to establishment of circulation (Fish and Wythe, 2015). For example, during development, Ephrin-B2 and its receptor EphB4 are exclusively expressed in arteries or veins, respectively (Wang et al., 1998; Adams et al., 1999; Gerety et al., 1999). Murine deletion of *Efnb2* or *EphB4* impairs A-V specification and causes A-V malformations (AVMs), high-flow vascular lesions characterized by direct connections of arteries to veins without intervening capillaries. A-V specification requires orchestrated activity of multiple signaling cascades (e.g., Eph-Ephrin, Hedgehog, vascular endothelial growth factor [VEGF], transforming growth factor β [TGF-β], and Notch) and transcriptional networks (e.g., Hes-related with YRPW motif [HEY] and Hairy Enhancer of Split [HES], Sry-related HMG box [SOX] factors, and COUP transcription factor 2 [COUP-TFII]) (Fish and Wythe, 2015). Nonetheless, the genetic determinants of A-V specification in humans remain incompletely understood.

During normal brain development, primitive choroidal and subependymal arteries that perfuse deep brain structures are connected via an intervening capillary network to the embryonic precursor of the vein of Galen (i.e., the median prosencephalic vein of Markowski [MPV]). The MPV returns deep cerebral venous blood to dural sinuses that drain into the internal jugular veins (Raybaud et al., 1989). Vein of Galen malformations (VOGMs), the most common and severe neonatal brain AVMs (Long et al., 1974; Deloison et al., 2012), directly connect primitive choroidal or subependymal cerebral arteries to the MPV, exposing it to dangerously high blood flow and pressures that can result in high-output cardiac failure, hydrocephalus, and/or brain hemorrhage (Recinos et al., 2012). VOGMs are also often associated with neurodevelopmental delay and congenital heart defects (CHDs) (McElhinney et al., 1998). Although endovascular partial obliteration of anomalous A-V connections has improved VOGM outcomes (Mitchell et al., 2001; Altschul et al., 2014), many VOGMs remain refractory to intervention, which is also inaccessible to many patients.

Limited knowledge of the molecular pathophysiology of VOGMs has hindered development of early diagnostic and targeted therapeutic strategies. Considered isolated, sporadic congenital lesions, rare VOGMs have been associated with Mendelian disorders, including 8 cases of autosomal dominant (AD) capillary malformation-AVM syndrome type 1 (CM-AVM1), caused by *RASA1* mutation (OMIM: 608354) (Revencu et al., 2013); 2 cases of AD CM-AVM syndrome type 2 (CM-AVM2), caused by *EPHB4* mutation (Amyere et al., 2017); and single cases of AD hereditary hemorrhagic telangiectasia type 1 (HHT1) because of *ENG* mutation (OMIM: 187300) (Tsutsumi et al., 2011) and AD HHT type 2 (HHT2), caused by *ACVRL1* mutation (OMIM: 600376, 1 case) (Chida et al., 2013).

Traditional genetic approaches have been limited in their ability to identify additional causative genes for VOGM because cases are rare and most often sporadic (Xu et al., 2010). This limitation motivates application of whole-exome sequencing (WES) to large numbers of affected subjects and their families, searching for genes mutated in probands more often than expected by chance. This unbiased approach has aided the study of other genetically heterogeneous neurodevelopmental disorders (Vissers et al., 2010; O'Roak et al., 2011, 2012; de Ligt et al., 2012; Iossifov et al., 2012; Neale et al., 2012;Rauch et al., 2012; Sanders et al., 2012; Allen et al., 2013; Iossifov et al., 2014; Krumm et al., 2015; Timberlake et al., 2016, 2017; Willsey et al., 2017), including those associated with brain malformations (Bilgüvar et al., 2010; Barak et al., 2011; Mishra-Gorur et al., 2014; Nikolaev et al., 2018), CHDs (Zaidi et al., 2013; Homsy et al., 2015; Jin et al., 2017), and congenital hydrocephalus (Furey et al., 2018). We hypothesized that VOGMs might arise from damaging *de novo* mutation events or incomplete penetrance of rare transmitted variants.

RESULTS

VOGM Cohort Characteristics and WES

We recruited 55 probands with radiographically confirmed VOGMs (STAR Methods) treated by endovascular therapy, including 52 parent-offspring trios with a single affected offspring and 3 singleton cases. 62% of probands were diagnosed prenatally or within 1 month after birth; only one was diagnosed after age 2. Common features at diagnosis included high-output cardiac failure (62%), macrocephaly (64%), hydrocephalus (60%), and prominent face and/or scalp vasculature (49%). Among the CHDs found in 9% were partial anomalous pulmonary venous return, patent *ductus arteriosus*, and pulmonary valve stenosis. Table S1 summarizes cohort demographics, clinical features, and radiographic classification, including angio-architectural subgroups (Lasjaunias et al., 2006). 37 of the 55 patients in our cohort presented with ''choroidal''-type lesions, defined as VOGMs with numerous feeder vessels and ''pseudoniduses'' that communicate with the MPV (Lasjaunias et al., 2006). The remaining 18 probands presented with ''mural'' VOGMs, characterized by fewer vessels of larger caliber that fistulize into the MPV (Lasjaunias et al., 2006). See Figure S1 for representative VOGM images.

DNA was isolated, and WES was performed as previously described (Timberlake et al., 2016). WES of 1,789 control trios comprising parents and unaffected siblings of autism probands was analyzed (Fischbach and Lord, 2010; Krumm et al., 2015) by our in-house informatics pipeline. In both cases and controls, 94.6% or more of targeted bases had 8 or more independent reads, and 89.8% or more had 15 or more independent reads (see Table S2 for exome metrics). Variant calling was performed utilizing the Genome Analysis Toolkit (GATK) HaplotypeCaller (McKenna et al., 2010; Van der Auwera et al., 2013) and allele frequency annotation by the Exome Aggregation Consortium (ExAC) and the Genome Aggregation Database (gnomAD) (Lek et al., 2016; STAR Methods). *De novo* mutation identification was performed by TrioDeNovo (Wei et al., 2015). MetaSVM was used to infer the effect of missense mutations (Dong et al., 2015). Missense variants were considered damaging (referred to as D-mis), when predicted to be deleterious by MetaSVM. Inferred loss-of-function (LoF) mutations, including stop gains, stop losses, frameshift insertions and deletions, and canonical splice site mutations were also considered damaging. Mutations

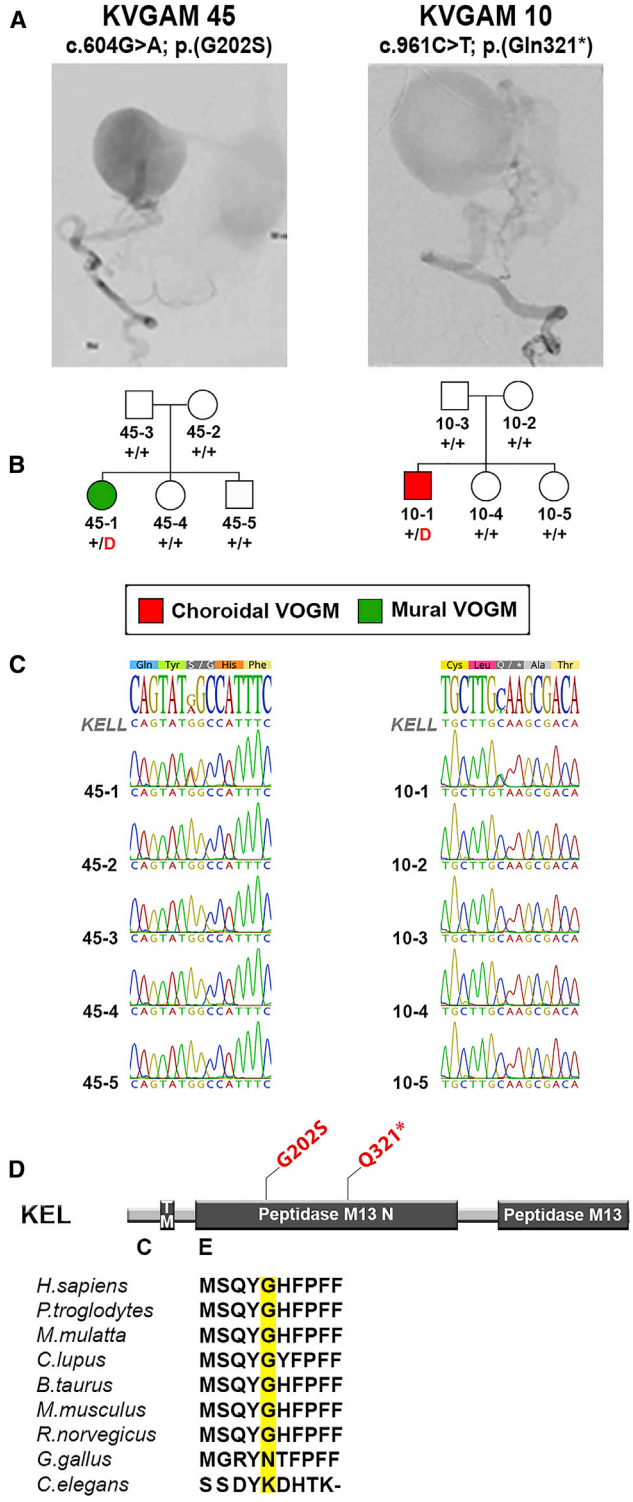

Figure 1. Protein-Altering *De Novo KEL* Mutations in VOGM

(A) Representative digital subtraction angiography images demonstrating mural and choroidal VOGMs in KVGAM45-1 and KVGAM10-1, respectively.

(B) Pedigrees depicting kindred structures. Note that probands carrying *de novo* mutations in *KEL* are the only members of families KVGAM45 and KVGAM10 with VOGMs; none of the family members in these two families have any disease phenotypes or cutaneous manifestations. A red D denotes protein-altering mutation; + denotes a wild-type sequence.

(C) Mutations identified by exome sequencing were confirmed by direct PCR amplification with custom primers followed by Sanger sequencing.

(D) Linear representation of the KEL polypeptide, with functional domains shown as dark rectangles. Amino acid modifications are mapped (in red) on the protein structure. Conservation of the wild-type amino acid substituted by the missense mutations is depicted below. TM, transmembrane domain.

in genes of interest were validated by PCR amplification and Sanger sequencing (Figure S2).

Enrichment in Damaging *De Novo* Mutations in VOGM Probands

The *de novo* mutation rate in probands was 1.56×10^{-8} per base pair, with 1.21 *de novo* coding region mutations per proband (Table S3), consistent with expectations and prior results (Homsy et al., 2015; Ware et al., 2015; Timberlake et al., 2017). The total *de novo* mutation burden in controls was also as reported previously (Timberlake et al., 2017). The distribution of types of *de novo* coding mutations in probands was compared with that expected from the probability of mutation of each base in the coding region and flanking splice sites (Samocha et al., 2014). Although synonymous mutations and inferred tolerated missense (T-mis) mutations in probands were not significantly enriched, *de novo* D-mis mutations in probands were marginally enriched ($p = 0.01$; enrichment = 2.05-fold; Table S3). In contrast, control subjects displayed no enrichment in any class of coding region mutation (Table S3). The observed excess of damaging *de novo* mutations in probands over that expected predicts that these mutations contribute to ~13% of VOGM cases.

One gene, *KEL*, exhibited more than one protein-altering *de novo* mutation (Figure 1). Among the 52 trios analyzed, we observed a near-significant enrichment of protein-altering *de novo* mutations in *KEL* (one-tailed *Poisson* test, $p = 4.2 \times 10^{-6}$; Benjamini-Hochberg false discovery rate [BH-FDR] = 0.08). One of these mutations caused premature termination (p.Gln321*), and the other was a missense mutation, p.Gly202Ser (Combined Annotation Dependent Depletion [CADD] = 22.6), both affecting the KELL polypeptide's peptidase domain (Figure 1).

We analyzed the burden of *de novo* mutations in genes highly intolerant to heterozygous LoF mutation (LoF-intolerant genes; probability of being loss-of-function intolerant [pLI] $\geq$ 0.9) (Lek et al., 2016), consistent with loss of one gene copy markedly impairing reproductive fitness. *De novo* D-mis mutations were marginally enriched (6 mutations; $p = 0.02$; enrichment = 2.82-fold; Table 1), of which four (3 D-mis and the only LoF mutation) occurred in genes encoding chromatin modifiers (*KMT2D*, *SMARCA2*, *SIRT1*, and *KAT6A*) (Figure 2). The 547 genes in the chromatin modifier gene ontology term GO:0016569 include 272 LoF-intolerant chromatin modifier genes; mutations in this set are enriched ($p = 8.9 \times 10^{-4}$; enrichment = 9.63-fold; Table 1), but *de novo* mutations in the LoF-intolerant chromatin modifier gene set were not enriched in controls (Table 1). A case-control analysis using the two-tailed binomial exact test (Sanders et al., 2012; Willsey et al., 2017) further supported this result (Table S4). In an orthogonal analysis of all genes using the permutation-based test (1 million iterations), the probability of finding 4 or

CellPress

Please cite this article in press as: Duran et al., Mutations in Chromatin Modifier and Ephrin Signaling Genes in Vein of Galen Malformation, Neuron (2018), https://doi.org/10.1016/j.neuron.2018.11.041

Table 1. Enrichment of Damaging *De Novo* Mutations in Chromatin Modifiers Intolerant to LoF Mutation in VOGM

Cases, n = 52							Controls, n = 1,789						
	Observed		Expected					Observed		Expected			
	N	Rate	N	Rate	Enrichment	*p*		N	Rate	N	Rate	Enrichment	*p*
LoF-Intolerant Genes (n = 3,230)													
Total	14	0.27	15.6	0.30	0.90	0.69	Total	504	0.28	527	0.29	0.96	0.85
Syn	2	0.04	4.3	0.08	0.46	0.93	Syn	127	0.07	145.6	0.08	0.87	0.95
Mis	11	0.21	9.8	0.19	1.12	0.39	Mis	339	0.19	331.7	0.19	1.02	0.33
D-Mis	6	0.12	2.1	0.04	2.82	0.02	D-Mis	64	0.04	72.7	0.04	0.88	0.86
LoF	1	0.02	1.5	0.03	0.69	0.77	LoF	38	0.02	49.7	0.03	0.76	0.96
Damaging	7	0.13	3.6	0.07	1.96	0.07	Damaging	102	0.06	122.4	0.07	0.83	0.97
All Chromatin Genes (n = 547)													
Total	4	0.08	2.3	0.04	1.73	0.20	Total	65	0.04	78.3	0.04	0.83	0.94
Syn	0	0.00	NA	NA	NA	NA	Syn	12	0.01	21.3	0.01	0.56	0.99
Mis	3	0.06	1.5	0.03	2.06	0.18	Mis	47	0.03	49.4	0.03	0.95	0.65
D-Mis	3	0.06	0.3	0.01	8.80	5.12×10^{-03}	D-Mis	12	0.01	11.6	0.01	1.03	0.50
LoF	1	0.02	0.2	3.85×10^{-03}	4.53	0.20	LoF	6	3.35×10^{-03}	7.6	4.25×10^{-03}	0.80	0.76
Damaging	4	0.08	0.6	0.01	7.12	2.66×10^{-03}	Damaging	18	0.01	19.2	0.01	0.94	0.64
Intolerant Chromatin Genes (n = 272)													
Total	4	0.08	1.6	0.03	2.56	0.07	Total	47	0.03	52.7	0.03	0.89	0.80
Syn	0	0.00	NA	NA	NA	NA	Syn	9	0.01	14.2	0.01	0.63	0.95
Mis	3	0.06	1	0.02	3.04	0.08	Mis	35	0.02	33.3	0.02	1.05	0.41
D-Mis	3	0.06	0.3	0.01	11.40	2.48×10^{-03}	D-Mis	7	3.91×10^{-03}	9	0.01	0.78	0.79
LoF	1	0.02	0.2	3.85×10^{-03}	6.55	0.14	LoF	3	1.68×10^{-03}	5.2	2.91×10^{-03}	0.58	0.89
Damaging	4	0.08	0.4	0.01	9.63	8.91×10^{-04}	Damaging	10	0.01	14.2	0.01	0.71	0.90

LoF, loss of function; N, the number of *de novo* mutations; rate, the number of *de novo* mutations divided by the number of individuals in the cohort; enrichment, ratio of observed to expected numbers of mutations; intolerant genes, genes with a pLI $\geq$ 0.9; D-Mis, damaging missense mutations as predicted by MetaSVM; damaging, D-Mis + LoF. Chromatin genes used for analysis were extracted from the Biomart database using GO:0016569 as the input. NA, not applicable.

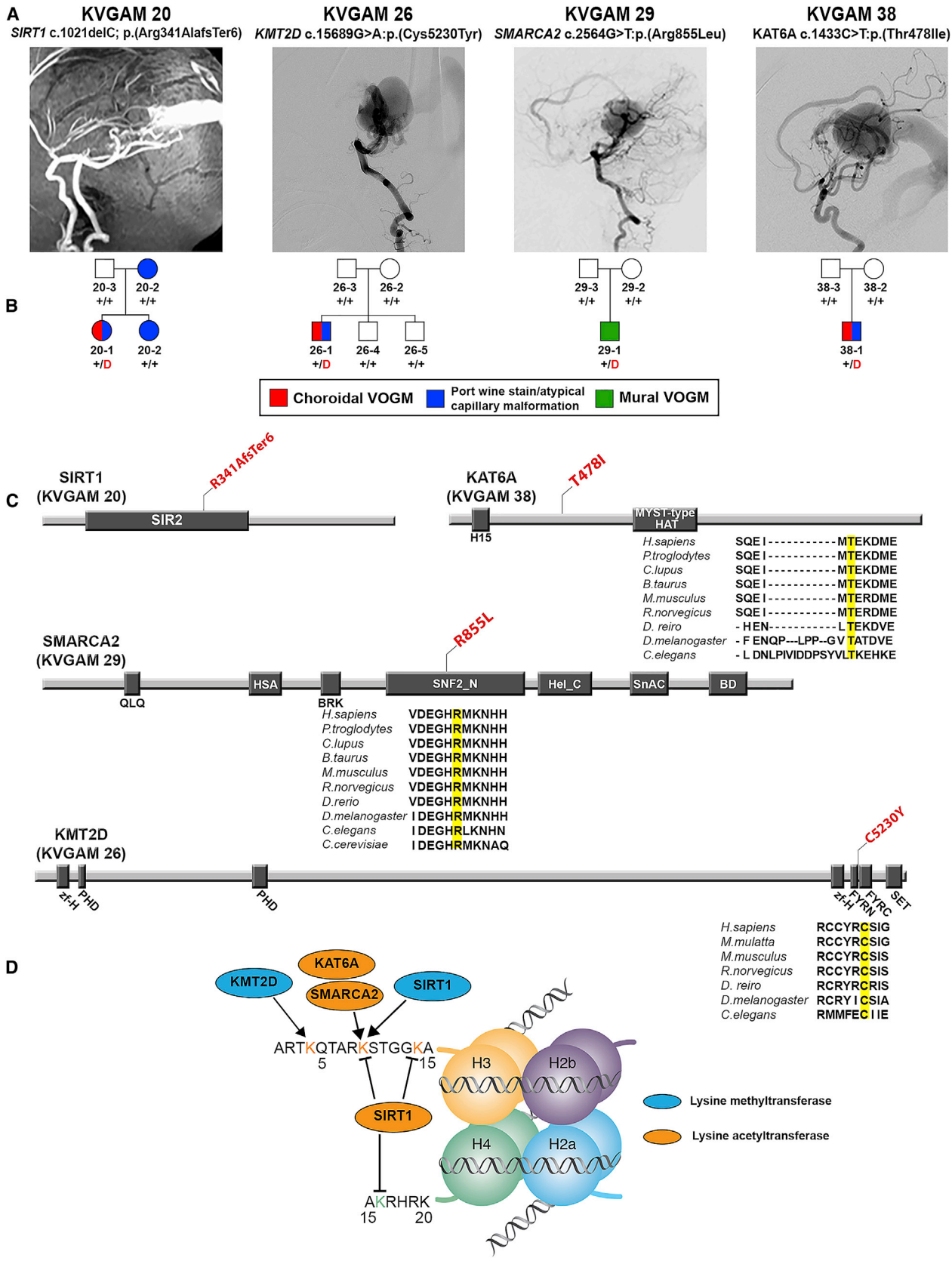

(legend on next page)

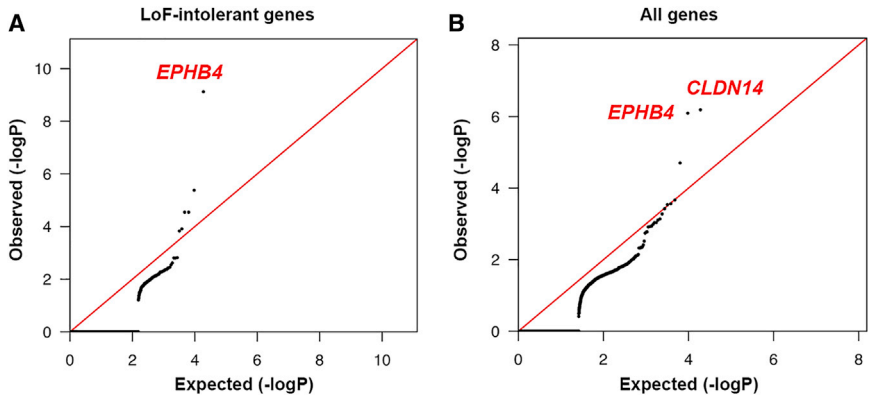

Figure 3. Exome-Wide Significant Enrichment of Rare Damaging Transmitted Mutations in *EPHB4* and *CLDN14*

(A) Quantile-quantile plots of observed versus expected binomial test p values for rare damaging (D-mis+LoF) variants with MAF $\leq 2 \times 10^{-5}$ in the Genome Aggregation database (gnomAD) in LoF-intolerant genes (pLI ≥ 0.9).

(B) Quantile-quantile plots of observed versus expected binomial test p values for rare damaging (D-mis+LoF) variants with MAF $\leq 2 \times 10^{-5}$ in gnomAD for all genes. MAF, minor allele frequency; D-mis, missense mutations predicted to be deleterious per MetaSVM; LoF, canonical loss-of-function mutations (stop gains, stop losses, frameshift insertions or deletions, and canonical splice site mutations).

more damaging *de novo* mutations in LoF-intolerant chromatin modifiers among a total of only 19 damaging *de novo* mutations in all genes was also low (empirical p = 3.5×10^{-3}; expected number = 0.66; STAR Methods). Damaging *de novo* mutations in chromatin modifiers were thus identified in ~7% of all VOGM probands (Table S5). Missense mutations occur in key functional domains of the encoded proteins at positions conserved through worm (*KAT6A* and *KMT2D*) and yeast (*SMARCA2*) (Figure 2C; Table S5). The clinical characteristics of probands harboring these mutations are shown in Figure 2 and Table S5.

Enrichment of Rare Damaging Transmitted Mutations in *EPHB4*

We next assessed the total burden in all probands of rare (minor allele frequency [MAF] $\leq 2 \times 10^{-5}$) *de novo* and transmitted D-mis and LoF mutations in LoF-intolerant genes (STAR Methods). The probability of the observed number of rare variants in each gene occurring by chance was calculated by comparing the observed with the expected burden, adjusting for gene lengths (Besse et al., 2017). Analysis of damaging variants in LoF-intolerant genes revealed genome-wide significant enrichment (Bonferroni multiple testing threshold = 2.63×10^{-6}) of mutations only in *EPHB4* (pLI = 0.99), with one LoF and three independent D-mis mutations (one-tailed binomial p = 7.47×10^{-10}; BH-FDR = 2.40×10^{-6}; enrichment = 341.13-fold; Figure 3A; Table 2).

Independent case-control gene burden analyses for damaging variants in all probands versus a cohort of 3,578 autism parental and ExAC controls showed a significant mutation burden in *EPHB4* versus autism parental controls (one-tailed Fisher's p = 1.68×10^{-6}, odds ratio = 89.97, 95% confidence interval [CI] [19.29, infinite [Inf]]) and versus ExAC controls (one-tailed Fisher's p = 1.98×10^{-6}, odds ratio = 49.76, 95% CI [16.39, Inf]); Table S6). The Bonferroni-corrected threshold for the 3,230 LoF-intolerant genes, 1.55×10^{-5}, was also surpassed by the *CAD* gene (one-tailed binomial p = 4.17×10^{-6}; BH-FDR = 0.01; enrichment = 101.08-fold).

All *EPHB4* mutations were transmitted; three of these are not observed in ExAC and gnomAD, and one has a MAF of 1.13×10^{-5} in gnomAD. All D-mis mutations in *EPHB4* alter highly conserved amino acid residues (Figure 4C; Table 2). Mutations p.Lys650Asn and p.Phe867Leu lie in the tyrosine kinase domain of the vein-specific (Gerety et al., 1999) Eph-B4 receptor. p.Ala509Gly lies in one of two EphB4 extracellular fibronectin III domains believed to bind the extracellular matrix (Figure 4C).

7 additional family members without diagnosed VOGM in these kindreds carried the same mutations. However, three *EPHB4* mutation carriers exhibited uncommon cutaneous vascular lesions. For example, in kindred VGAM-115, the mutation-carrying father had an abdominal port wine stain, and the proband's mutation carrier sibling had atypical left cheek and posterior thigh capillary malformations (Figures S3A and S3B). Similarly, the mutation-carrying mother in kindred KVGAM-33 had an atypical capillary malformation on her left arm, and the proband's mutation carrier sibling had an atrial septal defect (Figure 4B). Vascular and cardiac abnormalities were absent among non-mutation carriers in these families. All VOGMs associated with *EPHB4* mutations were of the choroidal subtype

Figure 2. Damaging *De Novo* Mutations in Chromatin Modifiers in VOGM

(A) Magnetic resonance angiographies and a digital subtraction angiography reconstruction demonstrating VOGM in probands from four pedigrees.

(B) Pedigree structures of VOGM kindreds. For each kindred, the gene and mutation, angiographic image, and pedigree structure are shown. Subjects with atypical capillary malformations are denoted by blue symbols. A red D denotes a damaging mutation; + denotes a wild-type sequence.

(C) Linear representation of functional domains of SIRT1, KMT2D, SMARCA2, and KAT6A with location of VOGM mutations. Functional domains are represented by dark rectangles. Amino acid changes (red) are located on the protein structure. For missense mutations, phylogenetic conservation of the wild-type amino acid is shown, with the mutated amino acid shown in yellow. SIR2, sirtuin catalytic domain, SIR2 domain; PHD, zinc finger PHD type; MOZ_SAS, histone acetyltransferase domain, MYST-type; zf-H, PHD-like zinc binding domain; FYRN, F/Y-rich domain – F/Y-rich N terminus motif; FYRC, F/Y-rich domain – F/Y-rich C terminus motif; SET, Su(var)3-9, enhancer-of-zeste and trithorax; QLQ, glutamine-leucine-glutamine domain; HAS, helicase-SANT-associated domain; BRK, BRK domain; SNF2_N, SNF2-related, N-terminal domain; Hel_C, helicase C-terminal domain; SnAC, Snf2-ATP coupling, chromatin remodeling complex; BD, bromodomain.

(D) Schematic of histone mark modifications by SIRT1, KMT2D, SMARCA2, and KAT6A.

Table 2. Transmitted Mutations in *EPHB4* and *CLDN14* in VOGM

Family	Type of VOGM	Ethnicity	Gene	Mutation	Domain Affected	ExAC MAF*	gnomAD MAF*	pLI	MetaSVM	CADD
VGAM115	choroidal	European	*EPHB4*	p.(Glu432fs1)	N/A	<9.06E−06	<4.76E−06	0.99	NA	N/A
KVGAM25	choroidal	European	*EPHB4*	p.(Ala509Gly)	fibronectin III	3.30E−05	1.13E−05	0.99	D	25
KVGAM33	choroidal	Mexican	*EPHB4*	p.(Lys650Asn)	tyrosine kinase	<8.24E−06	<4.06E−06	0.99	D	29.9
KVGAM18	choroidal	European	*EPHB4*	p.(Phe867Leu)	tyrosine kinase	<9.03E−06	<5.17E−06	0.99	D	31
VGAM100	choroidal	Mexican	*CLDN14*	p.(Ala113Pro)	second intracellular segment	<8.37E−06	8.28E−06	0	D	24.2
KVGAM20	choroidal	European	*CLDN14*	p.(Val143Met)	second extracellular segment	9.43E−06	1.24E−05	0	D	31
KVGAM51	mural	European	*CLDN14*	p.(Val143Met)	second extracellular segment	9.43E−06	1.24E−05	0	D	31

*For variants not observed in public databases, their minor allele frequency is calculated as less than 1 of the total number of alleles sampled at the closest locus with allele number available.

(Figures 4A and 4B). Together, these findings provide evidence of incomplete penetrance and variable expressivity of *EPHB4* mutations. Interestingly, 2 of 54 CM-AVM2 patients with *EPHB4* mutations also had VOGMs (Amyere et al., 2017).

Wild-type and VOGM mutant Eph-B4 (p.Ala509Gly; p.Lys650Asn; p.Phe867Leu) were expressed in mammalian cells (STAR Methods), and levels of Eph-B4 tyrosine (Tyr) phosphorylation, an index of tyrosine kinase activity (Lisabeth et al., 2013; Ferguson et al., 2015), were compared. The Eph-B4 kinase domain mutants p.Lys650Asn and p.Phe867Leu showed reduced or absent phosphorylation, respectively (Figure 4D). In contrast, the extracellular fibronectin III domain mutant p.Ala509Gly showed unchanged phosphorylation.

Eph-B4 Tyr phosphorylation creates docking sites for signaling molecules via a phosphotyrosine-SH2 domain interaction, facilitating Eph-B4 downstream signaling (Pawson and Scott, 1997; Wang et al., 2002). *RASA1*-encoded Ras GTPase-activating protein 1 (Ras-GAP) binds to these docking sites and regulates downstream signaling pathways (Kawasaki et al., 2014; Roth Flach et al., 2016). We immunoprecipitated wild-type or VOGM mutant Eph-B4 from mammalian cells co-expressing Ras-GAP. Ras-GAP co-immunoprecipitation with *EPHB4* mutant p.Lys650Asn was reduced, and Ras-GAP failed to bind Eph-B4 mutant p.Phe867Leu (Figure 4E). In contrast, wild-type Eph-B4 and Eph-B4 p.Ala509Gly bound Ras-GAP with similar affinity. These results are consistent with the cytoplasmic mutations impairing receptor kinase activity. The extracellular mutation alters the fibronectin domains, likely affecting signaling by altering binding to extracellular matrix ligands (a hypothesis not yet tested).

Recurrent Rare Damaging Transmitted Mutations in *CLDN14*

Expansion of the analysis to include the burden of rare (MAF $\leq 2 \times 10^{-5}$) D-mis and LoF mutations in all genes identified one additional gene, *CLDN14*, with a genome-wide significant damaging mutation burden (one-tailed binomial $p = 6.44 \times 10^{-7}$; BH-FDR = 0.01; enrichment = 190-fold; Figure 3B; Table 2). Comparing *CLDN14* mutation burden by case-control analysis against both autism parental controls (odds ratio = Inf, 95% CI [38.42, Inf]; one-tailed Fisher's $p = 3.38 \times 10^{-6}$; Table S6A) and ExAC controls (odds ratio = 67.82, 95% CI [17.66, Inf]; one-tailed Fisher's $p = 1.65 \times 10^{-5}$; Table S6B) supported the significance of this finding. The three rare damaging *CLDN14* mutations were all heterozygous transmitted missense mutations (5.5% of probands; Figure 5). Two are identical (p.Val143Met), present in unrelated VOGM probands, and are not observed in non-Finnish Europeans in ExAC. Beagle v3.3.2 kinship analysis (Browning and Browning, 2011; Stuart et al., 2015) and trio analysis using 139 phased genotypes flanking the mutation revealed that the p.Val143Met variant lies on a segment shared identically by descent from a common ancestor by the two probands, with a minimum shared segment of 0.34 Mb. Nonetheless, these probands shared no other rare variants, indicating that they do not share a recent common ancestor. The other rare damaging variant, p.Ala113Pro, is absent in ExAC, with MAF 8.28×10^{-6} in gnomAD.

CLDN14 encodes Claudin-14, a tight junction protein expressed in epithelia and endothelial cells of the brain and kidneys (Kniesel and Wolburg, 2000; Wattenhofer et al., 2005). Claudin extracellular loops make homo- or heterotypic interactions with adjacent cells to form the tight junction barrier (Van Itallie and Anderson, 2013). p.Val143Met alters a highly conserved residue in the second extracellular loop of Claudin-14 and is predicted to be deleterious by MetaSVM, CADD, PolyPhen2, and sorting tolerant from intolerant (SIFT). p.Ala113Pro lies in the second intracellular loop of Claudin-14 (Figure 5C; Figure S4).

Interestingly, in one of the families (KVGAM20) harboring the recurrent Claudin-14 mutation p.Val143Met, cutaneous vascular lesions segregated with the mutation among family members. The mother who transmitted the mutation had a port wine stain on her left thigh, and her children (proband and carrier sibling) had similar atypical capillary malformations in the nuchal area. This VOGM proband also had a midline atypical capillary malformation on her lower back (Figures S3G–S3J).

Enrichment of Mutations in Genes in the Ephrin Signaling Pathway

To search for pathways enriched for rare damaging mutations in VOGM, LoF-intolerant genes harboring damaging *de novo*

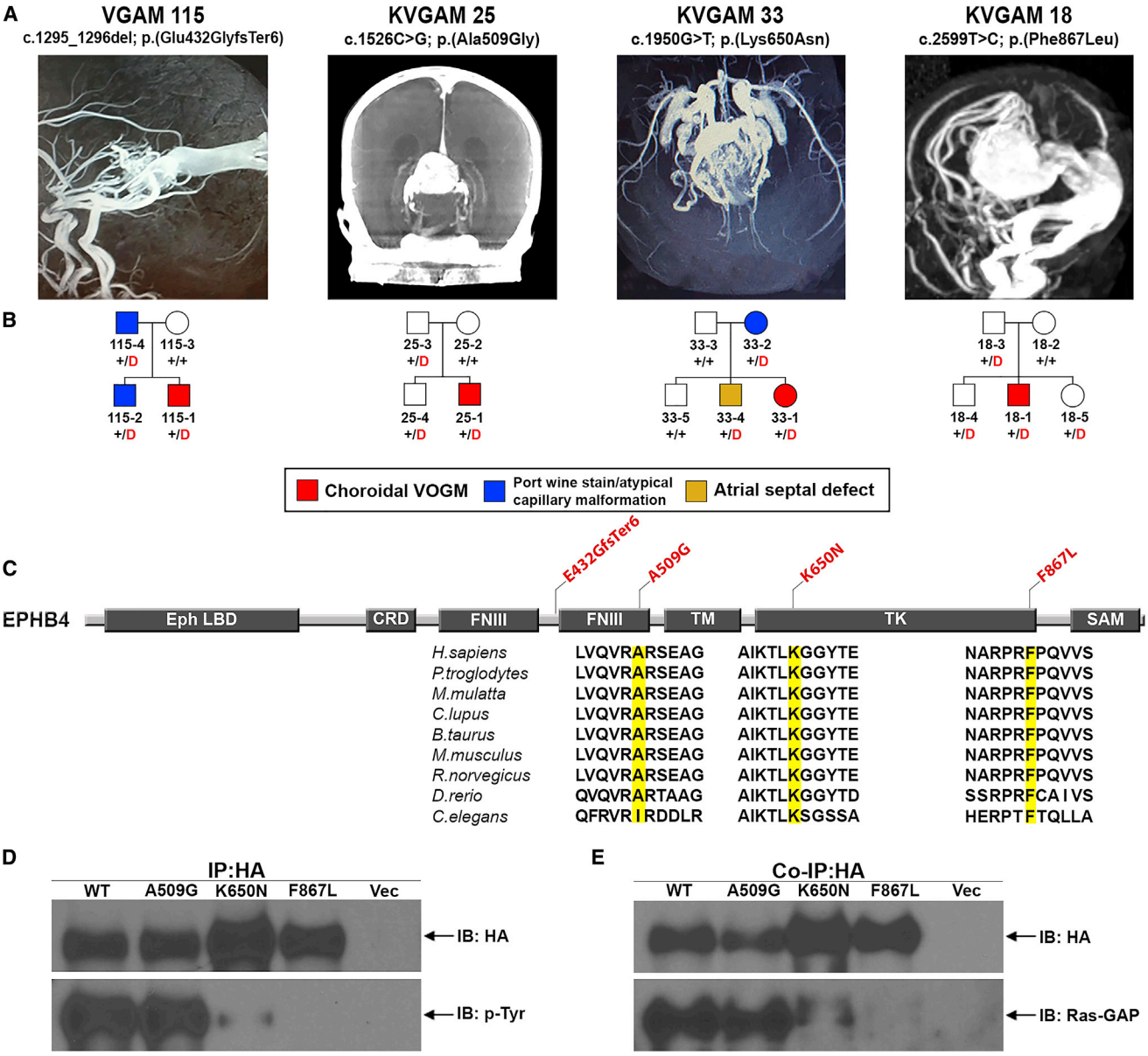

Figure 4. Damaging *EPHB4* Mutations in Choroidal VOGM

(A) Vascular imaging of probands from coronal reconstruction of computed tomography and magnetic resonance angiography demonstrating VOGMs.

(B) Pedigree structures of the kindreds, showing gene, mutation, and angiographic image. A carrier with an atrial septal defect in family KVGAM33 is shown in yellow. A red D denotes a damaging mutation; + denotes a wild-type sequence.

(C) Eph-B4 functional domains (dark rectangles) with location of VOGM mutations (red) and phylogenetic conservation of wild-type amino acid (yellow) at each mutated position. LB, ligand binding domain; CRD, cysteine-rich domain; FNIII, fibronectin III domain; TK, tyrosine kinase domain; SAM, sterile alpha motif.

(D) Representative immunoblots showing the effects of Ala509Gly, Lys650Asn, and Phe867Leu mutations on resting-state Eph-B4 tyrosine phosphorylation in HEK293T cells, analyzed by immunoprecipitation (IP) with hemagglutinin (HA) tag antibody followed by immunoblot (IB) with anti-p-tyrosine (p-Tyr) and HA tag antibodies. The blot demonstrates reduced p-Tyr content in Lys650Asn, with none detectable in Phe867Leu. Also shown is a representative immunoblot demonstrating binding of Eph-B4 constructs by Ras-GTPase-activating protein (GAP).

(E) Ras-GAP protein was co-immunoprecipitated with Eph-B4 mutants. Ras-GAP binding to Lys650Asn and to Phe867 was markedly reduced and abrogated, respectively.

and/or rare (MAF $\leq 2 \times 10^{-5}$) damaging transmitted mutations, along with *KEL* and *CLDN14*, were entered into Ingenuity Pathway Analysis (IPA; May 2018 version; total 128 input genes) (Krämer et al., 2014). Axonal guidance signaling, essential for vascular patterning and regulated by Ephrin-Eph receptor signaling (Adams and Eichmann, 2010), was the most significantly enriched canonical pathway ($p = 6.61 \times 10^{-8}$; BH-FDR = 1.33×10^{-5}), including Ephrin receptor signaling pathway

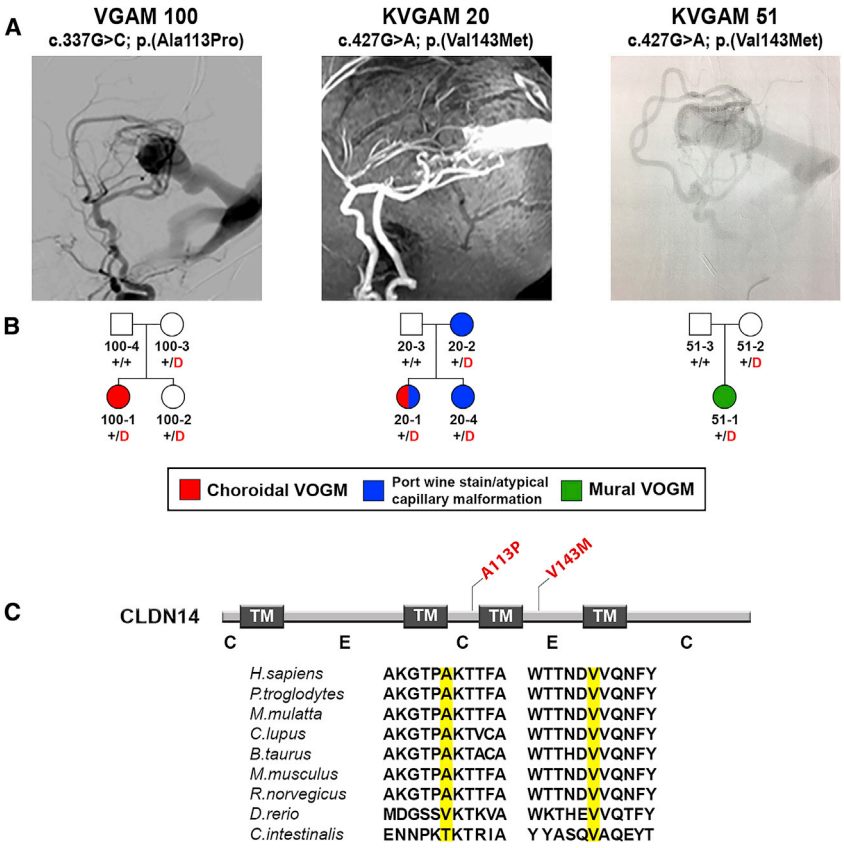

Figure 5. Damaging *CLDN14* Mutations in VOGM

(A) Representative images from digital subtraction angiographies and magnetic resonance angiography, demonstrating VOGMs of the probands.

(B) Pedigree structures indicating genotypes and phenotypes as described in Figure 2.

(C) Linear representation of Claudin-14 functional domains (dark rectangles) with location of VOGM mutations (red). Conservation of the wild-type amino acid is shown. C, cytoplasmic loop; E, extracellular loop.

genes (also significant). Nine additional IPA pathways were significant after Benjamini-Hochberg (B-H) correction (Table S7). Because IPA does not adjust for gene length, we tested each of these pathways in the case-control analysis (STAR Methods) using ethnicity-matched autism parents and ExAC controls. Axonal guidance and Ephrin receptor signaling pathways showed significant enrichment in cases (Table S8).

We further analyzed mutation burden in genes in these two pathways by binomial test, comparing observed with expected values as corrected for gene size (STAR Methods). Significant enrichment in both axonal guidance and Ephrin receptor signaling pathways was observed in cases, whereas analyses of synonymous variants in cases as well as rare damaging variants in autism parents and ExAC controls showed no significant enrichment (Table S9). Last, we found that most of the signal in the axonal guidance pathway was attributable to the Ephrin receptor signaling pathway because, after removal from analysis of the latter genes, the axonal guidance pathway was no longer significantly enriched (Table S10). Detailed variant information of damaging mutations in genes that contributed to the significant result is described in Table S11.

Of note, *EFNB2* (pLI = 0.94), encoding the Eph-B4 ligand Ephrin-B2, harbored the rare D-mis mutation p.Arg277His in a neonate with a choroidal VOGM (Figure S5). *EFNB2* is represented in the IPA axonal guidance and Ephrin receptor signaling gene sets, but this specific *EFNB2* variant was not included as input in our pathway analysis because its MAF slightly exceeded our threshold of 2×10^{-5} (MAF of 1.88×10^{-5} and 2.89×10^{-5} in ExAC and gnomAD, respectively). The proband's *EFNB2* mutation-carrying mother, although not having VOGM, exhibited multiple atypical nuchal capillary malformations. Of note, *Ephrin-b2* knockout mice phenocopy *eph-b4* knockout mice, exhibiting CNS and systemic AVMs, defects in cerebral angiogenesis, and embryonic lethality (Wang et al., 2010b).

Rare Damaging Mutations in Genes Implicated in Mendelian AVM Syndromes

VOGM is a rare feature in patients with CM-AVM types 1 and 2 because of mutation in *RASA1* (Revencu et al., 2013; Duran et al., 2018) and *EPHB4* (Amyere et al., 2017), respectively. VOGM has also previously been associated with single cases of HHT type 1 because of *ENG* mutation (Tsutsumi et al., 2011) and HHT type 2 because of *ACVRL1* mutation (OMIM: 600376) (Chida et al., 2013).

Our VOGM cohort included no *ENG* mutations. We found one damaging mutation in *RASA1* (p.Arg709*; Table S11), encoding the Eph-B4 binding partner and effector Ras GTPase-activating protein 1 (Ras-GAP) (Kawasaki et al., 2014), in a patient with a mural VOGM. This patient and mutation have been reported previously (Revencu et al., 2013) and was independently ascertained in the present study.

A single patient with a choroidal VOGM had a damaging p.Arg484Gln mutation in *ACVRL1* (Table S12), encoding ALK1, a receptor kinase in the TGF-β signaling pathway highly expressed in developing human vasculature (Zhang et al., 2017). This mutation, altering a conserved residue in the ALK1 kinase domain, was reported in HHT2 with isolated pulmonary hypertension (ClinVar: RCV000198604.1 and rs863223408) (Harrison et al., 2005). However, neither the *ACVRL1* mutant VOGM proband nor family members carrying the mutation exhibited HHT-associated findings (e.g., epistaxis or telangiectasia) or other vascular abnormalities. *ACVRL1* (ALK1) is a known regulator of Ephrin-B2-Eph-B4 signaling (Zhang, 2009; Kim et al., 2012; Roman and Hinck, 2017), and *acvrl1* deficient mice exhibit markedly enlarged cerebral vessels with A-V shunting and altered Eph-B4 expression (Walker et al., 2011).

Unrelated probands with mural VOGMs carried two rare damaging mutations (p.Gly39Ser and p.Asn373Ser) in the *ACVRL1* paralog *ACVR1* (pLI = 0.96; Table S12; Figures S6A and S6B), a gene not previously implicated in VOGM. The *ACVR1* p.Asn373Ser VOGM proband also had an atrial septal defect and partial anomalous pulmonary venous return (Figure S6B), and two mutation carriers in the family had cutaneous capillary malformations (Figure S6B). Neither the proband nor other family members had common HHT features (Abdalla et al., 2003). *ACVR1* encodes the receptor serine-threonine receptor kinase ALK2 coordinating with TGF-β type 2 receptors and co-receptors such as Endoglin (*ENG*) (Chen et al., 1998; Barbara et al., 1999; Wolfe and Myers, 2010). p.Gly39Ser alters a conserved residue in the extracellular ligand binding domain (Figure S6C). p.Asn373Ser alters a conserved residue predicted to be structurally critical for the cytoplasmic serine-threonine kinase (Figures S6D and S6E).

DISCUSSION

The rarity and the sporadic nature of VOGM have hindered its genetic understanding. This study, the largest trio-based genomic analysis of VOGM to date, has provided the following novel insights. First, probands exhibit an excess of damaging *de novo* mutations (~13% of cases); among these, mutations in chromatin modifier genes with essential roles in brain and heart development are enriched and inferred to affect ~8% of cases. Second, there is a prevalence of rare inherited damaging mutations in the Ephrin signaling genes, including a genome-wide significant burden in *EPHB4* (another ~16% of probands). Third, inherited mutations show incomplete penetrance and variable expressivity, with mutation carriers often exhibiting cutaneous vascular lesions, suggesting a two-hit mechanism. Thus, although rare mutations of large effect contribute to a significant fraction of VOGM cases, mutations in many additional genes likely contribute to disease pathogenesis. Our results support this hypothesis, suggesting potential pathogenic roles for *de novo KEL* mutations and rare inherited *CLDN14* mutations. However, the small number of observations and lack of replication studies require validation and extension by larger follow-up studies. Of note, analysis of rare homozygous and compound heterozygous genotypes (MAF $\leq$ 0.001) revealed no genes with more than one such genotype. See Table S13 for proband information and identified likely pathogenic mutations.

Genes encoding covalent histone modifiers and chromatin remodelers have been implicated in autism (De Rubeis et al., 2014), CHD (Jin et al., 2017), congenital hydrocephalus (Furey et al., 2018), and other congenital disorders (Feinberg, 2018). In our cohort, 4 of 55 probands had *de novo* mutations in chromatin modifiers. Enrichment of these mutations in our cohort and the conservation of the mutated residues in critical domains of protein function are consistent with each of these mutations contributing to VOGM pathogenesis. All four genes (*KMT2D*, *SMARCA2*, *SIRT1*, and *KAT6A)* are highly expressed in the developing human and murine brain (Machida et al., 2001; Ogawa et al., 2011; Pollen et al., 2015; Tham et al., 2015) and essential for neuronal and/or vascular development (Potente et al., 2007; Griffin et al., 2008; Van Laarhoven et al., 2015). *SMARCA2*, *KAT6A*, and *KMT2D* are mutated in Mendelian diseases that feature intellectual disability and/or epilepsy (Morin et al., 2003; Dentici et al., 2015). Mendelian phenotypes associated with *KAT6A* and *KMT2D* mutations include vascular defects and CHD (Arboleda et al., 2015; Van Laarhoven et al., 2015). Multiple mutated chromatin modifiers are shared among patients with CHD and autism (Zaidi et al., 2013; Homsy et al., 2015; Jin et al., 2017). ~87% of CHD patients with LoF *de novo* mutations in chromatin modifier genes exhibit neurodevelopmental phenotypes (Jin et al., 2017). These observations suggest that neurodevelopmental phenotypes in VOGM patients currently attributed to secondary CNS damage may, instead, reflect primary impairment from genetic mutation.

The role of Eph-B4 in A-V specification is well established in model systems (Zhang and Hughes, 2006; Mosch et al., 2010). Heterozygous missense variants in *EPHB4* have also been reported in two families with non-immune *hydrops fetalis* and/or atrial septal defect (HFASD; OMIM: 617300) (Martin-Almedina et al., 2016) and 54 families with CM-AVM2, featuring isolated cutaneous capillary malformations (63%) and associated AVMs (35%) (Amyere et al., 2017). We found damaging mutations in *EPHB4* in 7% of VOGM probands in this cohort. Two of 52 prior CM-AVM2 patients with *EPHB4* mutations were reported to have VOGMs (Amyere et al., 2017). During preparation of this manuscript, (Vivanti et al., 2018) reported 3 transmitted damaging mutations in *EPBH4* among WESs from 19 VOGM case-parent trios and two additional mutations from targeted sequencing of 32 other singleton VOGM probands. *Eph-b4* antisense morpholino knockdown in zebrafish embryos disrupts the angioarchitecture of the dorsal longitudinal vein, the homolog of the human vein of Galen precursor (Aurboonyawat et al., 2007). We conclude that heterozygous *EPHB4* germline mutations contribute to a spectrum of vascular pathology and that *EPHB4* is a *bona fide* VOGM risk gene.

Our analysis also demonstrated enrichment of rare heterozygous damaging mutations in Ephrin signaling genes (Table S11). These genes are expressed in the embryonic human brain and vasculature (Guo et al., 2012), regulate neurovascular development, and can be mapped into a single experimentally supported Search Tool for the Retrieval of Interacting Genes/Proteins (STRING) interactome (Figure S7; STAR Methods). Cutaneous vascular lesions are a common hallmark of developmental vascular disorders such as *RASA1*- and *EPHB4*-mutated CM-AVM (Revencu et al., 2013; Amyere et al., 2017), *ENG1*- and *ACVRL1*-mutated HHT (Chida et al., 2013), and *RASA1*-mutated Parkes Weber syndrome (Brouillard and Vikkula, 2007). We found similar cutaneous vascular lesions in VOGM kindreds harboring mutations in *EFNB2*, *EPHB4*, *EPHA4*, *ACVR1*, and *CLDN14*. These findings further implicate these genes in an Eph-B4-RASA1 signaling network (Figure S8).

Transmitted VOGM-associated mutations show incomplete penetrance. Moreover, many of the identified VOGM-associated genes harboring damaging *de novo* and inherited mutations have been implicated in other Mendelian diseases, sometimes producing different phenotypes. These observations highlight the pleiotropy with variable expressivity resulting from these mutations. These features have been described in other diseases. For example, haploinsufficiency for the identical chromatin

modifier genes results in CHD (Zaidi et al., 2013) or autism (Iossifov et al., 2014) or both. Variable expressivity of VOGM and associated features could arise from environmental modifiers (Stuart et al., 2015) in concert with the rare mutations identified and/or specific genetic modifiers (Timberlake et al., 2016). Co-mutation of genes in KVGAM20, VGAM100, and KVGAM45 could be important in this regard (Table S13). Sequencing additional exomes from VOGM kindreds will help clarify this issue.

The mechanisms by which syndromes characterized by abnormal A-V specification present with multifocal distributions of lesions remains poorly understood. Because 68% of VOGM families with full clinical data had capillary malformations or other uncommon cutaneous vascular lesions and that identified mutations in probands were found in all family members with these cutaneous lesions provides evidence linking VOGM and the cutaneous lesions to the same mutations (Table S13). This is consistent with a two-hit mechanism in which phenotypic expression relies on an inherited mutation and a second, post-zygotic mutation in the other wild-type allele (Brouillard et al., 2002; Pagenstecher et al., 2009). This mechanism has been shown for other hereditary multifocal vascular malformations, such as *RASA1*-mutated CM-AVM1 (Revencu et al., 2013), glomuvenous malformations (OMIM: 138000), cutaneomucosal venous malformation (OMIM: 600195), and cerebral cavernous malformations (OMIM: 116860) (Pagenstecher et al., 2009). In this context, phenotypic expression depends on the cell types in which somatic mutations occur and could explain the low penetrance of VOGM arising from transmitted mutations. Further work, including exome sequencing of lesional VOGM tissue, will test this hypothesis.

Although the identified *de novo KEL* mutations and inherited *CLDN14* mutations will require further validation by WES of additional VOGM patients and functional studies, several observations suggest the importance of the current findings. *KEL*, encoding the Kell blood group transmembrane glycoprotein, was the only gene in our study that harbored more than one protein-altering *de novo* mutation (Figure 1). Both the premature termination and p.Gly202Ser mutations in Kell alter its peptidase domain, shown to generate vasoactive endothelin peptides via cleavage of the endothelin-3 pro-protein (Lee et al., 1999). Endothelins provide vasculature-derived axonal guidance cues (Makita et al., 2008) involved in Ephrin-dependent vascular patterning (Adams and Eichmann, 2010).

CLDN14 was the only other gene besides *EPHB4* with genome-wide significant enrichment of transmitted damaging mutations. Recessive LoF genotypes in *CLDN14* cause sensorineural deafness type 29 (OMIM: 614035); in contrast, VOGM-associated *CLDN14* mutations are heterozygous and D-mis and include a recurrent missense mutation, suggesting gain-of-function or neomorphic effects and phenotypic heterogeneity. Claudin-14 is a tight junction protein in brain epithelia and endothelial cells (Kniesel and Wolburg, 2000; Wattenhofer et al., 2005). The regulation of tight junction formation by Claudins can affect endothelial cell permeability, integrity, and proliferation (Morita et al., 1999; González-Mariscal et al., 2007). The recurrent VOGM-associated Claudin-14 mutation lies in the large second extracellular loop that likely plays a role in tight junction formation. Endothelial cells heterozygous, but not homozygous, for *CLDN14* exhibit disruption of ZO-1-positive cell-cell junctions, abnormal distribution of basement membrane laminin, increased VEGF-stimulated angiogenesis, and significantly enhanced cell proliferation, suggesting a gene dosage effect (Baker et al., 2013). Functional interactions have been reported between Claudins and Ephrin-B2-EphB4 bi-directional signaling (Tanaka et al., 2005). In support of a possible Ephrin-Claudin-14 interaction is the fact that one of the families harboring the recurrent Claudin-14 mutation p.Val143Met had CM-AVM-like cutaneous vascular lesions that segregated with the mutation in family members (Figure 5B). The role of Claudin-14 in potential EphB4-dependent A-V specification will be a topic of future investigation.

These findings suggest that mutation carrier offspring may be at increased risk of VOGMs as well as capillary malformations and potentially other AVMs. However, not all mutation carriers develop capillary malformations, making absence of capillary malformations an unreliable clinical marker for transmission risk in affected families. These observations suggest the importance of family history and mutation-based screening for risk assessment. The narrow developmental window of gestational weeks 6–11 during which pulmonary vascular malformation (PVM) fistulas form (Raybaud et al., 1989) poses a challenge to improved early therapeutic strategies for VOGM. Thus, attempted diagnosis with intention to treat must occur before the safe gestational age threshold for amniocentesis (Shulman et al., 1994). These difficulties highlight the need for continued genetic research on VOGM with a focus on mechanistic implications of recently discovered VOGM-associated mutations.

Eph-B4 kinase domain mutations remove inhibition of downstream RAS-mitogen-activated protein kinase (MAPK)-ERK1/2 and phosphoinositide 3-kinase (PI3K)-AKT-mTORC1 signaling cascades (Kim et al., 2002; Salaita and Groves, 2010; Xiao et al., 2012). We showed that select VOGM-associated Eph-B4 mutations result in decreased binding of Eph-B4 to RASA1 (Figure 4E). PI3K-AKT-mTORC1 upregulation has been noted in capillary malformations of *RASA1* mutant CM-AVM1 patients (Kawasaki et al., 2014). Therapy targeting Eph-B4-Ras-GAP-mTOR signaling may represent a viable therapeutic approach for VOGM- and, perhaps, CM-AVM-spectrum lesions.

STAR★METHODS

Detailed methods are provided in the online version of this paper and include the following:

- KEY RESOURCES TABLE
- CONTACT FOR REAGENT AND RESOURCE SHARING
- EXPERIMENTAL MODEL AND SUBJECT DETAILS
  - Pateint Subjects
  - Whole Exome Sequencing and Variant Calling
- METHOD DETAILS
  - Kinship Analysis
  - De Novo Mutation Expectation Model
  - De Novo Enrichment Analysis and Variant Stratification
- QUANTIFICATION AND STATISTICAL ANALYSIS
  - Estimation of the Number of Damaging *De Novo* Mutations in LoF-intolerant Chromatin Modifiers

SUPPLEMENTAL INFORMATION

Supplemental Information includes eight figures and thirteen tables and can be found with this article online at https://doi.org/10.1016/j.neuron.2018.11.041.

ACKNOWLEDGMENTS

We thank the patients and families who participated in this research. We acknowledge support from the Yale-NIH Center for Mendelian Genomics (5U54HG006504) and an NIH NRCDP award to K.T.K. S.C.J. was supported by a James Hudson Brown-Alexander Brown Coxe postdoctoral fellowship and an American Heart Association postdoctoral fellowship. J.G. was supported by a Howard Hughes Institute medical research fellowship. Last, we acknowledge Collin Whitmore and his family for their inspiration, courage, and generous support.

AUTHOR CONTRIBUTIONS

Conceptualization, D.D. and K.T.K.; Methodology, D.D., X.Z., S.C.J., J.C., Q.L., R.P.L, and K.T.K.; Software, X.Z., S.C.J., J.C., C.G.F., Q.L., A.T.T., W.D., and S.H.; Validation, D.D., C.N.-W., J.G., and A.A.; Formal Analysis, D.D., X.Z, S.C.J., J.C., Q.L, M.S., and S.H.; Investigation, D.D., X.Z, S.C.J., J.C., C.N.-W., B.Y., W.D., M.A.S., E.L., J.K., A.A., A.H., J.K.K., M.W.Y., J.Z., M.L.D., C.C.M., S.M., I.R.T., C.C., F.L.-G., J.K., S.H., M.S., S.L.A., M.K., A.F.D., J.M.Z., A.D., B.P.W., C.J.S., B.A.-K., G.R., E.J., E.R.S., D.B.O., A.B., K.B., M.V., M.G., R.P.L., and K.T.K.; Resources, C.N.-W., C.C.M., S.M., M.K., A.F.D., B.A.-K., J.M.Z., A.D., C.S., B.P.W., G.R., E.J., E.R.S, D.O., M.V., A.B., K.B., R.P.L., and K.T.K.; Data Curation, D.D., X.Z., S.C.J., J.C., C.G.F., and A.T.T.; Writing – Original Draft, D.D., X.Z., S.C.J., J.C., R.P.L., and K.T.K.; Writing – Review & Editing, D.D., X.Z., S.C.J., J.C., C.G.F., A.T.T., Q.L., S.L.A., R.P.L., and K.T.K.; Visualization, D.D.; Supervision, R.P.L., and K.T.K.; Project Administration, D.D., X.Z., S.C.J., J.C., R.P.L., and K.T.K.; Funding Acquisition, R.P.L. and K.T.K.

DECLARATION OF INTERESTS

The authors declare no competing interests.

Received: June 14, 2018
Revised: October 12, 2018
Accepted: November 20, 2018
Published: December 18, 2018

REFERENCES

Abagyan, R., Totrov, M., and Kuznetsov, D. (1994). Icm - a New Method for Protein Modeling and Design - Applications to Docking and Structure Prediction from the Distorted Native Conformation. J. Comput. Chem. *15*, 488–506.

Abdalla, S.A., Geisthoff, U.W., Bonneau, D., Plauchu, H., McDonald, J., Kennedy, S., Faughnan, M.E., and Letarte, M. (2003). Visceral manifestations in hereditary haemorrhagic telangiectasia type 2. J. Med. Genet. *40*, 494–502.

Adams, R.H., and Eichmann, A. (2010). Axon guidance molecules in vascular patterning. Cold Spring Harb. Perspect. Biol. *2*, a001875.

Adams, R.H., Wilkinson, G.A., Weiss, C., Diella, F., Gale, N.W., Deutsch, U., Risau, W., and Klein, R. (1999). Roles of ephrinB ligands and EphB receptors in cardiovascular development: demarcation of arterial/venous domains, vascular morphogenesis, and sprouting angiogenesis. Genes Dev. *13*, 295–306.

Allen, A.S., Berkovic, S.F., Cossette, P., Delanty, N., Dlugos, D., Eichler, E.E., Epstein, M.P., Glauser, T., Goldstein, D.B., Han, Y., et al.; Epi4K Consortium; Epilepsy Phenome/Genome Project (2013). De novo mutations in epileptic encephalopathies. Nature *501*, 217–221.

Altschul, D., Paramasivam, S., Ortega-Gutierrez, S., Fifi, J.T., and Berenstein, A. (2014). Safety and efficacy using a detachable tip microcatheter in the embolization of pediatric arteriovenous malformations. Childs Nerv. Syst. *30*, 1099–1107.

Amyere, M., Revencu, N., Helaers, R., Pairet, E., Baselga, E., Cordisco, M., Chung, W., Dubois, J., Lacour, J.P., Martorell, L., et al. (2017). Germline Loss-of-Function Mutations in EPHB4 Cause a Second Form of Capillary Malformation-Arteriovenous Malformation (CM-AVM2) Deregulating RAS-MAPK Signaling. Circulation *136*, 1037–1048.

Apweiler, R., Bairoch, A., Wu, C.H., Barker, W.C., Boeckmann, B., Ferro, S., Gasteiger, E., Huang, H., Lopez, R., Magrane, M., et al. (2004). UniProt: the Universal Protein knowledgebase. Nucleic Acids Res. *32*, D115–D119.

Arboleda, V.A., Lee, H., Dorrani, N., Zadeh, N., Willis, M., Macmurdo, C.F., Manning, M.A., Kwan, A., Hudgins, L., Barthelemy, F., et al. (2015). De novo nonsense mutations in KAT6A, a lysine acetyl-transferase gene, cause a syndrome including microcephaly and global developmental delay. Am. J. Hum. Genet. *96*, 498–506.

Aurboonyawat, T., Suthipongchai, S., Pereira, V., Ozanne, A., and Lasjaunias, P. (2007). Patterns of cranial venous system from the comparative anatomy in vertebrates. Part I, introduction and the dorsal venous system. Interv. Neuroradiol. *13*, 335–344.

Baker, M., Reynolds, L.E., Robinson, S.D., Lees, D.M., Parsons, M., Elia, G., and Hodivala-Dilke, K. (2013). Stromal Claudin14-heterozygosity, but not deletion, increases tumour blood leakage without affecting tumour growth. PLoS ONE *8*, e62516.

Barak, T., Kwan, K.Y., Louvi, A., Demirbilek, V., Saygı, S., Tüysüz, B., Choi, M., Boyacı, H., Doerschner, K., Zhu, Y., et al. (2011). Recessive LAMC3 mutations cause malformations of occipital cortical development. Nat. Genet. *43*, 590–594.

Barbara, N.P., Wrana, J.L., and Letarte, M. (1999). Endoglin is an accessory protein that interacts with the signaling receptor complex of multiple members of the transforming growth factor-beta superfamily. J. Biol. Chem. *274*, 584–594.

Besse, W., Dong, K., Choi, J., Punia, S., Fedeles, S.V., Choi, M., Gallagher, A.R., Huang, E.B., Gulati, A., Knight, J., et al. (2017). Isolated polycystic liver disease genes define effectors of polycystin-1 function. J. Clin. Invest. *127*, 1772–1785.

Bilgüvar, K., Oztürk, A.K., Louvi, A., Kwan, K.Y., Choi, M., Tatli, B., Yalnizoğlu, D., Tüysüz, B., Cağlayan, A.O., Gökben, S., et al. (2010). Whole-exome sequencing identifies recessive WDR62 mutations in severe brain malformations. Nature *467*, 207–210.

Brouillard, P., and Vikkula, M. (2007). Genetic causes of vascular malformations. *16*, R140–R149.

Brouillard, P., Boon, L.M., Mulliken, J.B., Enjolras, O., Ghassibé, M., Warman, M.L., Tan, O.T., Olsen, B.R., and Vikkula, M. (2002). Mutations in a novel factor, glomulin, are responsible for glomuvenous malformations ("glomangiomas"). Am. J. Hum. Genet. *70*, 866–874.

Browning, B.L., and Browning, S.R. (2011). A fast, powerful method for detecting identity by descent. Am. J. Hum. Genet. *88*, 173–182.

Chen, Y.G., Hata, A., Lo, R.S., Wotton, D., Shi, Y., Pavletich, N., and Massagué, J. (1998). Determinants of specificity in TGF-beta signal transduction. Genes Dev. *12*, 2144–2152.

Chida, A., Shintani, M., Wakamatsu, H., Tsutsumi, Y., Iizuka, Y., Kawaguchi, N., Furutani, Y., Inai, K., Nonoyama, S., and Nakanishi, T. (2013). ACVRL1

gene variant in a patient with vein of Galen aneurysmal malformation. J. Pediatr. Genet. *2*, 181–189.

de Ligt, J., Willemsen, M.H., van Bon, B.W., Kleefstra, T., Yntema, H.G., Kroes, T., Vulto-van Silfhout, A.T., Koolen, D.A., de Vries, P., Gilissen, C., et al. (2012). Diagnostic exome sequencing in persons with severe intellectual disability. N. Engl. J. Med. *367*, 1921–1929.

DePristo, M.A., Banks, E., Poplin, R., Garimella, K.V., Maguire, J.R., Hartl, C., Philippakis, A.A., del Angel, G., Rivas, M.A., Hanna, M., et al. (2011). A framework for variation discovery and genotyping using next-generation DNA sequencing data. Nat. Genet. *43*, 491–498.

De Rubeis, S., He, X., Goldberg, A.P., Poultney, C.S., Samocha, K., Cicek, A.E., Kou, Y., Liu, L., Fromer, M., Walker, S., et al.; DDD Study; Homozygosity Mapping Collaborative for Autism; UK10K Consortium (2014). Synaptic, transcriptional and chromatin genes disrupted in autism. Nature *515*, 209–215.

Deloison, B., Chalouhi, G.E., Sonigo, P., Zerah, M., Millischer, A.E., Dumez, Y., Brunelle, F., Ville, Y., and Salomon, L.J. (2012). Hidden mortality of prenatally diagnosed vein of Galen aneurysmal malformation: retrospective study and review of the literature. Ultrasound Obstet. Gynecol. *40*, 652–658.

Dentici, M.L., Di Pede, A., Lepri, F.R., Gnazzo, M., Lombardi, M.H., Auriti, C., Petrocchi, S., Pisaneschi, E., Bellacchio, E., Capolino, R., et al. (2015). Kabuki syndrome: clinical and molecular diagnosis in the first year of life. Arch. Dis. Child *100*, 158–164.

Dong, C., Wei, P., Jian, X., Gibbs, R., Boerwinkle, E., Wang, K., and Liu, X. (2015). Comparison and integration of deleteriousness prediction methods for nonsynonymous SNVs in whole exome sequencing studies. Hum. Mol. Genet. *24*, 2125–2137.

Duran, D., Karschnia, P., Gaillard, J.R., Karimy, J.K., Youngblood, M.W., DiLuna, M.L., Matouk, C.C., Aagaard-Kienitz, B., Smith, E.R., Orbach, D.B., et al. (2018). Human genetics and molecular mechanisms of vein of Galen malformation. J. Neurosurg. Pediatr. *21*, 367–374.

Feinberg, A.P. (2018). The Key Role of Epigenetics in Human Disease Prevention and Mitigation. N. Engl. J. Med. *378*, 1323–1334.

Ferguson, B.D., Tan, Y.H., Kanteti, R.S., Liu, R., Gayed, M.J., Vokes, E.E., Ferguson, M.K., Iafrate, A.J., Gill, P.S., and Salgia, R. (2015). Novel EPHB4 Receptor Tyrosine Kinase Mutations and Kinomic Pathway Analysis in Lung Cancer. Sci. Rep. *5*, 10641.

Fischbach, G.D., and Lord, C. (2010). The Simons Simplex Collection: a resource for identification of autism genetic risk factors. Neuron *68*, 192–195.

Fish, J.E., and Wythe, J.D. (2015). The molecular regulation of arteriovenous specification and maintenance. Dev. Dyn. *244*, 391–409.

Fromer, M., and Purcell, S.M. (2014). Using XHMM Software to Detect Copy Number Variation in Whole-Exome Sequencing Data. Curr. Protoc. Hum. Genet. *81*, 1–21.

Furey, C.G., Choi, J., Jin, S.C., Zeng, X., Timberlake, A.T., Nelson-Williams, C., Mansuri, M.S., Lu, Q., Duran, D., Panchagnula, S., et al. (2018). De Novo Mutation in Genes Regulating Neural Stem Cell Fate in Human Congenital Hydrocephalus. Neuron *99*, 302–314.

Gerety, S.S., Wang, H.U., Chen, Z.F., and Anderson, D.J. (1999). Symmetrical mutant phenotypes of the receptor EphB4 and its specific transmembrane ligand ephrin-B2 in cardiovascular development. Mol. Cell *4*, 403–414.

Gerrard, D.T., Berry, A.A., Jennings, R.E., Piper Hanley, K., Bobola, N., and Hanley, N.A. (2016). An integrative transcriptomic atlas of organogenesis in human embryos. eLife *5*, e15657.

González-Mariscal, L., Lechuga, S., and Garay, E. (2007). Role of tight junctions in cell proliferation and cancer. Prog. Histochem. Cytochem. *42*, 1–57.

Griffin, C.T., Brennan, J., and Magnuson, T. (2008). The chromatin-remodeling enzyme BRG1 plays an essential role in primitive erythropoiesis and vascular development. Development *135*, 493–500.

Guo, S., Zhou, Y., Xing, C., Lok, J., Som, A.T., Ning, M., Ji, X., and Lo, E.H. (2012). The vasculome of the mouse brain. PLoS ONE *7*, e52665.

Harrison, R.E., Berger, R., Haworth, S.G., Tulloh, R., Mache, C.J., Morrell, N.W., Aldred, M.A., and Trembath, R.C. (2005). Transforming growth factor-beta receptor mutations and pulmonary arterial hypertension in childhood. Circulation *111*, 435–441.

Homsy, J., Zaidi, S., Shen, Y., Ware, J.S., Samocha, K.E., Karczewski, K.J., DePalma, S.R., McKean, D., Wakimoto, H., Gorham, J., et al. (2015). De novo mutations in congenital heart disease with neurodevelopmental and other congenital anomalies. Science *350*, 1262–1266.

Iossifov, I., Ronemus, M., Levy, D., Wang, Z., Hakker, I., Rosenbaum, J., Yamrom, B., Lee, Y.H., Narzisi, G., Leotta, A., et al. (2012). De novo gene disruptions in children on the autistic spectrum. Neuron *74*, 285–299.

Iossifov, I., O'Roak, B.J., Sanders, S.J., Ronemus, M., Krumm, N., Levy, D., Stessman, H.A., Witherspoon, K.T., Vives, L., Patterson, K.E., et al. (2014). The contribution of de novo coding mutations to autism spectrum disorder. Nature *515*, 216–221.

Jin, S.C., Homsy, J., Zaidi, S., Lu, Q., Morton, S., DePalma, S.R., Zeng, X., Qi, H., Chang, W., Sierant, M.C., et al. (2017). Contribution of rare inherited and de novo variants in 2,871 congenital heart disease probands. Nat. Genet. *49*, 1593–1601.

Kawasaki, J., Aegerter, S., Fevurly, R.D., Mammoto, A., Mammoto, T., Sahin, M., Mably, J.D., Fishman, S.J., and Chan, J. (2014). RASA1 functions in EPHB4 signaling pathway to suppress endothelial mTORC1 activity. J. Clin. Invest. *124*, 2774–2784.

Kim, I., Ryu, Y.S., Kwak, H.J., Ahn, S.Y., Oh, J.L., Yancopoulos, G.D., Gale, N.W., and Koh, G.Y. (2002). EphB ligand, ephrinB2, suppresses the VEGF- and angiopoietin 1-induced Ras/mitogen-activated protein kinase pathway in venous endothelial cells. FASEB J. *16*, 1126–1128.

Kim, J.H., Peacock, M.R., George, S.C., and Hughes, C.C. (2012). BMP9 induces EphrinB2 expression in endothelial cells through an Alk1-BMPRII/ActRII-ID1/ID3-dependent pathway: implications for hereditary hemorrhagic telangiectasia type II. Angiogenesis *15*, 497–509.

Kniesel, U., and Wolburg, H. (2000). Tight junctions of the blood-brain barrier. Cell. Mol. Neurobiol. *20*, 57–76.

Krämer, A., Green, J., Pollard, J., Jr., and Tugendreich, S. (2014). Causal analysis approaches in Ingenuity Pathway Analysis. Bioinformatics *30*, 523–530.

Krumm, N., Turner, T.N., Baker, C., Vives, L., Mohajeri, K., Witherspoon, K., Raja, A., Coe, B.P., Stessman, H.A., He, Z.X., et al. (2015). Excess of rare, inherited truncating mutations in autism. Nat. Genet. *47*, 582–588.

Lasjaunias, P.L., Chng, S.M., Sachet, M., Alvarez, H., Rodesch, G., and Garcia-Monaco, R. (2006). The management of vein of Galen aneurysmal malformations. Neurosurgery *59*, S184–S194.

Laskowski, R.A., Macarthur, M.W., Moss, D.S., and Thornton, J.M. (1993). Procheck - a Program to Check the Stereochemical Quality of Protein Structures. J. Appl. Crystallogr. *26*, 283–291.

Lee, S., Lin, M., Mele, A., Cao, Y., Farmar, J., Russo, D., and Redman, C. (1999). Proteolytic processing of big endothelin-3 by the kell blood group protein. Blood *94*, 1440–1450.

Lek, M., Karczewski, K.J., Minikel, E.V., Samocha, K.E., Banks, E., Fennell, T., O'Donnell-Luria, A.H., Ware, J.S., Hill, A.J., Cummings, B.B., et al.; Exome Aggregation Consortium (2016). Analysis of protein-coding genetic variation in 60,706 humans. Nature *536*, 285–291.

Li, H. (2014). Toward better understanding of artifacts in variant calling from high-coverage samples. Bioinformatics *30*, 2843–2851.

Li, H., and Durbin, R. (2010). Fast and accurate long-read alignment with Burrows-Wheeler transform. Bioinformatics *26*, 589–595.

Lisabeth, E.M., Falivelli, G., and Pasquale, E.B. (2013). Eph receptor signaling and ephrins. Cold Spring Harb. Perspect. Biol. *5*, a009159.

Long, D.M., Seljeskog, E.L., Chou, S.N., and French, L.A. (1974). Giant arteriovenous malformations of infancy and childhood. J. Neurosurg. *40*, 304–312.

Machida, Y., Murai, K., Miyake, K., and Iijima, S. (2001). Expression of chromatin remodeling factors during neural differentiation. J. Biochem. *129*, 43–49.

Makita, T., Sucov, H.M., Gariepy, C.E., Yanagisawa, M., and Ginty, D.D. (2008). Endothelins are vascular-derived axonal guidance cues for developing sympathetic neurons. Nature *452*, 759–763.

Manichaikul, A., Mychaleckyj, J.C., Rich, S.S., Daly, K., Sale, M., and Chen, W.M. (2010). Robust relationship inference in genome-wide association studies. Bioinformatics *26*, 2867–2873.

Martin-Almedina, S., Martinez-Corral, I., Holdhus, R., Vicente, A., Fotiou, E., Lin, S., Petersen, K., Simpson, M.A., Hoischen, A., Gilissen, C., et al. (2016). EPHB4 kinase-inactivating mutations cause autosomal dominant lymphatic-related hydrops fetalis. J. Clin. Invest. *126*, 3080–3088.

McElhinney, D.B., Halbach, V.V., Silverman, N.H., Dowd, C.F., and Hanley, F.L. (1998). Congenital cardiac anomalies with vein of Galen malformations in infants. Arch. Dis. Child. *78*, 548–551.

McKenna, A., Hanna, M., Banks, E., Sivachenko, A., Cibulskis, K., Kernytsky, A., Garimella, K., Altshuler, D., Gabriel, S., Daly, M., and DePristo, M.A. (2010). The Genome Analysis Toolkit: a MapReduce framework for analyzing next-generation DNA sequencing data. Genome Res. *20*, 1297–1303.

Mishra-Gorur, K., Çağlayan, A.O., Schaffer, A.E., Chabu, C., Henegariu, O., Vonhoff, F., Akgümüş, G.T., Nishimura, S., Han, W., Tu, S., et al. (2014). Mutations in KATNB1 cause complex cerebral malformations by disrupting asymmetrically dividing neural progenitors. Neuron *84*, 1226–1239.

Mitchell, P.J., Rosenfeld, J.V., Dargaville, P., Loughnan, P., Ditchfield, M.R., Frawley, G., and Tress, B.M. (2001). Endovascular management of vein of Galen aneurysmal malformations presenting in the neonatal period. AJNR Am. J. Neuroradiol. *22*, 1403–1409.

Morin, G., Villemain, L., Baumann, C., Mathieu, M., Blanc, N., and Verloes, A. (2003). Nicolaides-Baraitser syndrome: confirmatory report of a syndrome with sparse hair, mental retardation, and short stature and metacarpals. Clin. Dysmorphol *12*, 237–240.

Morita, K., Sasaki, H., Furuse, M., and Tsukita, S. (1999). Endothelial claudin: claudin-5/TMVCF constitutes tight junction strands in endothelial cells. J. Cell Biol. *147*, 185–194.

Mosch, B., Reissenweber, B., Neuber, C., and Pietzsch, J. (2010). Eph receptors and ephrin ligands: important players in angiogenesis and tumor angiogenesis. J. Oncol. *2010*, 135285.

Neale, B.M., Kou, Y., Liu, L., Ma'ayan, A., Samocha, K.E., Sabo, A., Lin, C.F., Stevens, C., Wang, L.S., Makarov, V., et al. (2012). Patterns and rates of exonic de novo mutations in autism spectrum disorders. Nature *485*, 242–245.

Nikolaev, S.I., Vetiska, S., Bonilla, X., Boudreau, E., Jauhiainen, S., Rezai Jahromi, B., Khyzha, N., DiStefano, P.V., Suutarinen, S., Kiehl, T.R., et al. (2018). Somatic Activating KRAS Mutations in Arteriovenous Malformations of the Brain. N. Engl. J. Med. *378*, 250–261.

O'Roak, B.J., Deriziotis, P., Lee, C., Vives, L., Schwartz, J.J., Girirajan, S., Karakoc, E., Mackenzie, A.P., Ng, S.B., Baker, C., et al. (2011). Exome sequencing in sporadic autism spectrum disorders identifies severe de novo mutations. Nat. Genet. *43*, 585–589.

O'Roak, B.J., Vives, L., Girirajan, S., Karakoc, E., Krumm, N., Coe, B.P., Levy, R., Ko, A., Lee, C., Smith, J.D., et al. (2012). Sporadic autism exomes reveal a highly interconnected protein network of de novo mutations. Nature *485*, 246–250.

Ogawa, T., Wakai, C., Saito, T., Murayama, A., Mimura, Y., Youfu, S., Nakamachi, T., Kuwagata, M., Satoh, K., and Shioda, S. (2011). Distribution of the longevity gene product, SIRT1, in developing mouse organs. Congenit. Anom. (Kyoto) *51*, 70–79.

Pagenstecher, A., Stahl, S., Sure, U., and Felbor, U. (2009). A two-hit mechanism causes cerebral cavernous malformations: complete inactivation of CCM1, CCM2 or CCM3 in affected endothelial cells. Hum. Mol. Genet. *18*, 911–918.

Pawson, T., and Scott, J.D. (1997). Signaling through scaffold, anchoring, and adaptor proteins. Science *278*, 2075–2080.

Pollen, A.A., Nowakowski, T.J., Chen, J., Retallack, H., Sandoval-Espinosa, C., Nicholas, C.R., Shuga, J., Liu, S.J., Oldham, M.C., Diaz, A., et al. (2015). Molecular identity of human outer radial glia during cortical development. Cell *163*, 55–67.

Potente, M., Ghaeni, L., Baldessari, D., Mostoslavsky, R., Rossig, L., Dequiedt, F., Haendeler, J., Mione, M., Dejana, E., Alt, F.W., et al. (2007). SIRT1 controls endothelial angiogenic functions during vascular growth. Genes Dev. *21*, 2644–2658.

Protack, C.D., Foster, T.R., Hashimoto, T., Yamamoto, K., Lee, M.Y., Kraehling, J.R., Bai, H., Hu, H., Isaji, T., Santana, J.M., et al. (2017). Eph-B4 regulates adaptive venous remodeling to improve arteriovenous fistula patency. Sci. Rep. *7*, 15386.

Rauch, A., Wieczorek, D., Graf, E., Wieland, T., Endele, S., Schwarzmayr, T., Albrecht, B., Bartholdi, D., Beygo, J., Di Donato, N., et al. (2012). Range of genetic mutations associated with severe non-syndromic sporadic intellectual disability: an exome sequencing study. Lancet *380*, 1674–1682.

Raybaud, C.A., Strother, C.M., and Hald, J.K. (1989). Aneurysms of the vein of Galen: embryonic considerations and anatomical features relating to the pathogenesis of the malformation. Neuroradiology *31*, 109–128.

Recinos, P.F., Rahmathulla, G., Pearl, M., Recinos, V.R., Jallo, G.I., Gailloud, P., and Ahn, E.S. (2012). Vein of Galen malformations: epidemiology, clinical presentations, management. Neurosurg. Clin. N. Am. *23*, 165–177.

Revencu, N., Boon, L.M., Mendola, A., Cordisco, M.R., Dubois, J., Clapuyt, P., Hammer, F., Amor, D.J., Irvine, A.D., Baselga, E., et al. (2013). RASA1 mutations and associated phenotypes in 68 families with capillary malformation-arteriovenous malformation. Hum. Mutat. *34*, 1632–1641.

Roman, B.L., and Hinck, A.P. (2017). ALK1 signaling in development and disease: new paradigms. Cell. Mol. Life Sci. *74*, 4539–4560.

Roth Flach, R.J., Guo, C.A., Danai, L.V., Yawe, J.C., Gujja, S., Edwards, Y.J., and Czech, M.P. (2016). Endothelial Mitogen-Activated Protein Kinase Kinase Kinase Kinase 4 Is Critical for Lymphatic Vascular Development and Function. Mol. Cell. Biol. *36*, 1740–1749.

Salaita, K., and Groves, J.T. (2010). Roles of the cytoskeleton in regulating EphA2 signals. Commun. Integr. Biol. *3*, 454–457.

Samocha, K.E., Robinson, E.B., Sanders, S.J., Stevens, C., Sabo, A., McGrath, L.M., Kosmicki, J.A., Rehnström, K., Mallick, S., Kirby, A., et al. (2014). A framework for the interpretation of de novo mutation in human disease. Nat. Genet. *46*, 944–950.

Sanders, S.J., Murtha, M.T., Gupta, A.R., Murdoch, J.D., Raubeson, M.J., Willsey, A.J., Ercan-Sencicek, A.G., DiLullo, N.M., Parikshak, N.N., Stein, J.L., et al. (2012). De novo mutations revealed by whole-exome sequencing are strongly associated with autism. Nature *485*, 237–241.

Schneider, C.A., Rasband, W.S., and Eliceiri, K.W. (2012). NIH Image to ImageJ: 25 years of image analysis. Nat. Methods *9*, 671–675.

Shulman, L.P., Elias, S., Phillips, O.P., Grevengood, C., Dungan, J.S., and Simpson, J.L. (1994). Amniocentesis performed at 14 weeks' gestation or earlier: comparison with first-trimester transabdominal chorionic villus sampling. Obstet. Gynecol. *83*, 543–548.

Stuart, B.D., Choi, J., Zaidi, S., Xing, C., Holohan, B., Chen, R., Choi, M., Dharwadkar, P., Torres, F., Girod, C.E., et al. (2015). Exome sequencing links mutations in PARN and RTEL1 with familial pulmonary fibrosis and telomere shortening. Nat. Genet. *47*, 512–517.

Szklarczyk, D., Franceschini, A., Wyder, S., Forslund, K., Heller, D., Huerta-Cepas, J., Simonovic, M., Roth, A., Santos, A., Tsafou, K.P., et al. (2015). STRING v10: protein-protein interaction networks, integrated over the tree of life. Nucleic Acids Res. *43*, D447–D452.

Tanaka, M., Kamata, R., and Sakai, R. (2005). EphA2 phosphorylates the cytoplasmic tail of Claudin-4 and mediates paracellular permeability. J. Biol. Chem. *280*, 42375–42382.

Tham, E., Lindstrand, A., Santani, A., Malmgren, H., Nesbitt, A., Dubbs, H.A., Zackai, E.H., Parker, M.J., Millan, F., Rosenbaum, K., et al. (2015). Dominant mutations in KAT6A cause intellectual disability with recognizable syndromic features. Am. J. Hum. Genet. *96*, 507–513.

Timberlake, A.T., Choi, J., Zaidi, S., Lu, Q., Nelson-Williams, C., Brooks, E.D., Bilguvar, K., Tikhonova, I., Mane, S., Yang, J.F., et al. (2016). Two locus inheritance of non-syndromic midline craniosynostosis via rare *SMAD6* and common *BMP2* alleles. eLife *5*, e20125.

Timberlake, A.T., Furey, C.G., Choi, J., Nelson-Williams, C., Yale Center for Genome Analysis, Loring, E., Galm, A., Kahle, K.T., Steinbacher, D.M.,

Larysz, D., et al. (2017). De novo mutations in inhibitors of Wnt, BMP, and Ras/ERK signaling pathways in non-syndromic midline craniosynostosis. Proc. Natl. Acad. Sci. U.S.A *114*, E7341–E7347.

Tsutsumi, Y., Kosaki, R., Itoh, Y., Tsukamoto, K., Matsuoka, R., Shintani, M., Nosaka, S., Masaki, H., and Iizuka, Y. (2011). Vein of Galen aneurysmal malformation associated with an endoglin gene mutation. Pediatrics *128*, e1307–e1310.

Van der Auwera, G.A., Carneiro, M.O., Hartl, C., Poplin, R., Del Angel, G., Levy-Moonshine, A., Jordan, T., Shakir, K., Roazen, D., Thibault, J., et al. (2013). From FastQ data to high confidence variant calls: the Genome Analysis Toolkit best practices pipeline. Curr. Protoc. Bioinformatics *43*, 11.10.1–33.

Van Itallie, C.M., and Anderson, J.M. (2013). Claudin interactions in and out of the tight junction. Tissue Barriers *1*, e25247.

Van Laarhoven, P.M., Neitzel, L.R., Quintana, A.M., Geiger, E.A., Zackai, E.H., Clouthier, D.E., Artinger, K.B., Ming, J.E., and Shaikh, T.H. (2015). Kabuki syndrome genes KMT2D and KDM6A: functional analyses demonstrate critical roles in craniofacial, heart and brain development. Hum. Mol. Genet. *24*, 4443–4453.

Venugopal, A. (2014). Disseminated intravascular coagulation. Indian J. Anaesth. *58*, 603–608.

Vissers, L.E., de Ligt, J., Gilissen, C., Janssen, I., Steehouwer, M., de Vries, P., van Lier, B., Arts, P., Wieskamp, N., del Rosario, M., et al. (2010). A de novo paradigm for mental retardation. Nat. Genet. *42*, 1109–1112.

Vivanti, A., Ozanne, A., Grondin, C., Saliou, G., Quevarec, L., Maurey, H., Aubourg, P., Benachi, A., Gut, M., Gut, I., et al. (2018). Loss of function mutations in EPHB4 are responsible for vein of Galen aneurysmal malformation. Brain *141*, 979–988.

Walker, E.J., Su, H., Shen, F., Choi, E.J., Oh, S.P., Chen, G., Lawton, M.T., Kim, H., Chen, Y., Chen, W., and Young, W.L. (2011). Arteriovenous malformation in the adult mouse brain resembling the human disease. Ann. Neurol. *69*, 954–962.

Wang, H.U., Chen, Z.F., and Anderson, D.J. (1998). Molecular distinction and angiogenic interaction between embryonic arteries and veins revealed by ephrin-B2 and its receptor Eph-B4. Cell *93*, 741–753.

Wang, Z., Miura, N., Bonelli, A., Mole, P., Carlesso, N., Olson, D.P., and Scadden, D.T. (2002). Receptor tyrosine kinase, EphB4 (HTK), accelerates differentiation of select human hematopoietic cells. Blood *99*, 2740–2747.

Wang, K., Li, M., and Hakonarson, H. (2010a). ANNOVAR: functional annotation of genetic variants from high-throughput sequencing data. Nucleic Acids Res. *38*, e164.

Wang, Y., Nakayama, M., Pitulescu, M.E., Schmidt, T.S., Bochenek, M.L., Sakakibara, A., Adams, S., Davy, A., Deutsch, U., Lüthi, U., et al. (2010b). Ephrin-B2 controls VEGF-induced angiogenesis and lymphangiogenesis. Nature *465*, 483–486.

Ware, J.S., Samocha, K.E., Homsy, J., and Daly, M.J. (2015). Interpreting de novo Variation in Human Disease Using denovolyzeR. Curr. Protoc. Hum. Genet. *87*, 7.25.1–15.

Wattenhofer, M., Reymond, A., Falciola, V., Charollais, A., Caille, D., Borel, C., Lyle, R., Estivill, X., Petersen, M.B., Meda, P., and Antonarakis, S.E. (2005). Different mechanisms preclude mutant CLDN14 proteins from forming tight junctions in vitro. Hum. Mutat. *25*, 543–549.

Wei, Q., Zhan, X., Zhong, X., Liu, Y., Han, Y., Chen, W., and Li, B. (2015). A Bayesian framework for de novo mutation calling in parents-offspring trios. Bioinformatics *31*, 1375–1381.

Wiederstein, M., and Sippl, M.J. (2007). ProSA-web: interactive web service for the recognition of errors in three-dimensional structures of proteins. Nucleic Acids Res. *35*, W407–410.

Willsey, A.J., Fernandez, T.V., Yu, D., King, R.A., Dietrich, A., Xing, J., Sanders, S.J., Mandell, J.D., Huang, A.Y., Richer, P., et al. (2017). De Novo Coding Variants Are Strongly Associated with Tourette Disorder. Neuron *94*, 486–499.e9.

Wolfe, J.M., and Myers, L. (2010). Fur in the midst of the waters: visual search for material type is inefficient. J. Vis. *10*, 8.

Xiao, Z., Carrasco, R., Kinneer, K., Sabol, D., Jallal, B., Coats, S., and Tice, D.A. (2012). EphB4 promotes or suppresses Ras/MEK/ERK pathway in a context-dependent manner: Implications for EphB4 as a cancer target. Cancer Biol. Ther. *13*, 630–637.

Xu, D.S., Usman, A.A., Hurley, M.C., Eddleman, C.S., and Bendok, B.R. (2010). Adult presentation of a familial-associated vein of galen aneurysmal malformation: case report. Neurosurgery *67*, E1845–E1851.

Zaidi, S., Choi, M., Wakimoto, H., Ma, L., Jiang, J., Overton, J.D., Romano-Adesman, A., Bjornson, R.D., Breitbart, R.E., Brown, K.K., et al. (2013). De novo mutations in histone-modifying genes in congenital heart disease. Nature *498*, 220–223.

Zhang, Y.E. (2009). Non-Smad pathways in TGF-beta signaling. Cell Res. *19*, 128–139.

Zhang, J., and Hughes, S. (2006). Role of the ephrin and Eph receptor tyrosine kinase families in angiogenesis and development of the cardiovascular system. J. Pathol. *208*, 453–461.

Zhang, J., Schwartz, M.P., Hou, Z., Bai, Y., Ardalani, H., Swanson, S., Steill, J., Ruotti, V., Elwell, A., Nguyen, B.K., et al. (2017). A Genome-wide Analysis of Human Pluripotent Stem Cell-Derived Endothelial Cells in 2D or 3D Culture. Stem Cell Reports *8*, 907–918.

STAR★METHODS

KEY RESOURCES TABLE

REAGENT or RESOURCE	SOURCE	IDENTIFIER
Deposited Data		
Whole exome sequencing data of 52 VOGM trios and 3 singletons	This paper	Accession number phs000744.v4.p2 https://www.ncbi.nlm.nih.gov/projects/gap/cgi-bin/study.cgi?study_id=phs000744
Whole exome sequencing data of 1,789 control trios from the Simon Simplex Collection	Iossifov et al., 2014	NDAR: https://doi.org/10.15154/1149697 https://ndar.nih.gov/study.html?id=352
Software and Algorithms		
Genome Analysis Tool Kit (GATK)	DePristo et al., 2011; McKenna et al., 2010; Van der Auwera et al., 2013	https://software.broadinstitute.org/gatk/best-practices/
BWA-mem	Li and Durbin, 2010	http://bio-bwa.sourceforge.net/
Annovar	Wang et al., 2010a	http://annovar.openbioinformatics.org/en/latest/
PLINK/SEQ	Fromer and Purcell, 2014	https://atgu.mgh.harvard.edu/plinkseq/
Antibodies		
Anti-Phosphotyrosine Monoclonal Antibody; P-Tyr-100	Cell Signaling Technology, Danvers, MA, USA	RRID: AB_331230
Anti-Ras GAP Monoclonal Antibody	Santa Cruz Biotechnology, Dallas, TX, USA	RRID: AB_628207
Anti-HA-Tag antibody	Cell Signaling Technology, Danvers, MA, USA	RRID: AB_10691311
Other		
1000 Genomes GRCh37 h19 genome build	1000 Genomes Project	http://ftp.1000genomes.ebi.ac.uk/vol1/ftp/technical/reference/human_g1k_v37.fasta.gz
RefSeq hg19 gene annotation	UCSC Genome Browser	http://genome.ucsc.edu/cgi-bin/hgTables?command=start
Intervals file for IDT xGen v1.0	Integrated DNA Technologies	http://www.idtdna.com/pages/products/next-generation-sequencing/hybridization-capture/lockdown-panels/xgen-exome-research-panel
ExAC Browser (Beta)	Exome Aggregation Consortium	http://exac.broadinstitute.org/
gnomAD Browser	genome Aggregation Database	http://gnomad-old.broadinstitute.org/

CONTACT FOR REAGENT AND RESOURCE SHARING

Further information and requests for resources and reagents should be directed to and will be fulfilled by the Lead Contact, Dr. Kristopher T. Kahle (kristopher.kahle@yale.edu).

EXPERIMENTAL MODEL AND SUBJECT DETAILS

Pateint Subjects

All procedures in this study comply with Yale University's Human Investigation Committee (HIC) and are Human Research Protection Program. Written informed consent was obtained from all adult participants. Parent or legal guardian authorization was obtained in writing for sample collection of all minors in this study. Inclusion criteria included male or female patients with clearly defined mural or choroidal VOGMs, radiographically-confirmed by both a neurosurgeon and neuroradiologist from an angiogram or magnetic resonance angiogram, along with their family members. Fifty-five probands diagnosed with VOGM were included in this study, of which 52 were parent-offspring trios. Among these 55 VOGM probands, 65.5% were female, 76.4% were self-reported Europeans, and 56.4% had a family history of cutaneous vascular abnormalities. (Table S1).

Controls consist of 1,789 unaffected sublings of autism cases and unaffected parents from the Simons Foundation Autism Research Initiative Simplex Collection (SSC)(Fischbach and Lord, 2010; O'Roak et al., 2011; Sanders et al., 2012; Iossifov et al., 2014; Krumm

et al., 2015). Only the unaffected siblings and parents, as designated by SSC, were included in the analysis and served as controls for this study. Permission to access to the genomic data in the SCC on the National Institute of Mental Health Data Repository was obtained. Written informed consent for all participants was provided by the Simons Foundation Autism Research Initiative.

Whole Exome Sequencing and Variant Calling

Exon capture was performed on genomic DNA samples derived from saliva or blood using Roche SeqCap EZ MedExome Target Enrichment kit or IDT xGen target capture kit followed by 99 base paired-end sequencing on the Illumina HiSeq 2500 platform. Sequence reads were aligned to the human reference genome GRCh37/hg19 using BWA-MEM (Li, 2014) and further processed to call variants following the GATK Best Practices workflow (McKenna et al., 2010). Variants were annotated with ANNOVAR (Wang et al., 2010a) and MetaSVM (Dong et al., 2015) was used to predict the deleteriousness of non-synonymous variants (herein referred to as D-mis). All variants covered by independent aligned sequencing reads with a depth of 8x or greater were visualized *in silico* to eliminate false positives.

De novo mutations were called using TrioDeNovo (Venugopal, 2014). Candidate *de novo* mutations were further filtered based on the following criteria: (1) exonic or splice-site variants; (2) read depth (DP) of 10 in the proband and both parents; (3) genotype quality (GQ) score $\geq$ 20; (4) minium proband alternative read depth of 5; (5) proband alternative allele ratio $\geq$ 28% if having < 10 alternative reads or $\geq$ 20% if having $\geq$ 10 alternative reads; (6) alternative allele ratio in both parents $\leq$ 3.5%; (8) in-cohort allele frequency $\leq 4 \times 10^{-4}$ for controls and MAF $\leq 4 \times 10^{-4}$ in gnomAD for cases due to limited cohort size.

For rare transmitted dominant variants, only LoF mutations (stop-gains, stop-losses, canonical splice-sites, and frameshift indels) and D-mis mutations (missense mutations predicted deleterious by MetaSVM) were considered potentially damaging for subsequent one-tailed binomial analysis and filtered using the following criteria to reduce false positives: (1) GATK variant quality score recalibration (VQSR) of PASS, (2) MAF $\leq 2 \times 10^{-5}$ in gnomAD (calculated based on combined dataset of WES and WGS data from gnomAD database, Lek et al., 2016), (3) DP $\geq$ 8 independent reads, and (4) GQ score $\geq$ 20. Transmitted recessive variants were filtered for rare (MAF $\leq 10^{-3}$ in gnomAD) homozygous and compound heterozygous variants using the same criteria described above.

Candidate mutations were confirmed by PCR amplification followed by Sanger sequencing (primer sequences available on request).

METHOD DETAILS

Kinship Analysis

Pairwise proband relatedness and pedigree information of trios were confirmed using KING (Manichaikul et al., 2010) by estimating kinship coefficient and calculating identity-by-descent (IBD). The shared pairwise IBD segments in 45 European probands were detected using Beagle v3.3.2 (Browning and Browning, 2011).

De Novo Mutation Expectation Model

We used a sequence context probability model to derive the per-gene probability of observing a *de novo* mutation by chance as previously described (Samocha et al., 2014). In brief, for each base in the exonic region, the probability of observing each of the three possible single nucleotide changes was determined. The coding consequence of each possible mutation was determined, and then these probabilities of mutations were summed for each variant functional class (synonymous, missense, nonsense, canonical splice site, frameshift, and stop-lost) to create a per-gene probability of mutations. The probability of a frameshift mutation was determined by multiplying the probability of a nonsense mutation by 1.25 as described previously (Samocha et al., 2014). In-frame insertions and deletions are not currently accounted for by this framework and were not included in the analysis. The per-gene probability for each functional class was adjusted to control for sequencing coverage. Due to the difference in exome capture kits, DNA sequencing platforms, and variable sequencing coverage between case and control cohorts, the expected number of *de novo* mutations was estimated by adjusting for sequencing depth in 52 case trios and 1,789 autism control trios separately.

De Novo Enrichment Analysis and Variant Stratification

Rather than using the variant calls in controls published in the SSC study (Krumm et al., 2015), we downloaded the bam files from the SSC, reanalyzed the data, and filtered the control v*cf.* file using the same filtering criteria as what was used in our case cohort. A one-tail Poisson test was used to compare observed number of *de novo* mutations across each variant class to expected number under the null hypothesis. R package 'denovolyzeR' (Ware et al., 2015) was used to perform the analyses. The Benjamini-Hochberg method was used to correct for multiple testing while taking into account all genes (n = 18,989) and calculate adjusted p values. A gene was considered significant if Benjamini-Hochberg adjusted p value is $\leq$ 0.05. All genes represented in this dataset were annotated with artery-specific and brain-specific expression values in a form of reads per kilobase transcript per million reads (RPKM) from the GTEx database (https://gtexportal.org/home/). Genes harboring *de novo* mutations were also annotated with human brain specific expression data obtained during the first four weeks of development (Gerrard et al., 2016) in the form of quantile rank based on transcript per kilobase million (TPM), indicating the relative rank of expression level within human genome. The final dataset was analyzed for

recurrently affected genes, and all variants in genes affected by a single *de novo* mutation were stratified. LoF variants were ranked based on pLI (from highest to lowest).

QUANTIFICATION AND STATISTICAL ANALYSIS

Estimation of the Number of Damaging *De Novo* Mutations in LoF-intolerant Chromatin Modifiers

One million permutations were performed to derive the empirical distribution of the number of damaging *de novo* mutation in the LoF-intolerant chromatin modifier genes. For each permutation, the number of observed damaging *de novo* mutations in all genes (n = 19) was randomly distributed across the exome, weighted according to the *de novo* probabilities of damaging mutations. The empirical p value is calculated as the proportion of times that the number of damaging *de novo* mutations in the LoF-intolerant chromatin modifier genes is greater than or equal to the observed number (n = 4). The average number of damaging *de novo* mutations in the LoF-intolerant chromatin modifier genes is also calculated.

Binomial Analysis

Independent binomial tests were used to compare the expected and observed counts of rare variants in each gene. The expected number of rare damaging variants is determined by taking the fractional length of a gene (in base pairs) relative to the entire exome and multiplying this by the total number of rare damaging variants. This represents the expected occurrence of sporadic mutations in each gene without considering the influences of selection pressure or precedents of ethnic background. Inputs for this test were those with inferred pathogenicity, including missense mutations called deleterious per MetaSVM and inferred LoF mutations (stop-gains, stop-losses, frameshift insertions and deletions, or canonical splice site mutations). Binomial analysis for mutational enrichment did not include non-frameshift insertions or deletions. The Benjamini-Hochberg method was performed taking into account all genes (n = 18,989 for *CLDN14*) or all LoF-intolerant genes (n = 3,230 for *EPHB4* and *CAD*) as described above and the significance cutoff was 0.05. We reported genes that reached a more stringent Bonferroni multiple testing cutoff of 2.63×10^{-6} (= 0.05/18,989) or 1.55×10^{-5} for binomial testing of all genes or LoF-intolerant genes, respectively.

Pathway Analysis

Inputs for this analysis were LoF-intolerant genes (pLI $\geq$ 0.9) harboring damaging *de novo* mutations and/or rare (MAF $\leq 2 \times 10^{-5}$) damaging transmitted mutations, as well as genes with significant burden of *de novo* (*KEL*) or transmitted mutation (*EPHB4* and *CLDN14*) (n = 128 genes) into Ingenuity Pathway Analysis (IPA, Apr 2018). Core analysis using Ingenuity Knowledge Base (Gene Only) as the reference set was performed. P value was calculated using a one-tailed Fisher's exact test reflecting the likelihood that the overlap between the input and a given gene set is due to random chance. In individual based case-control analysis, ethnicity-matched case and control samples were filtered using the same criteria. Individuals carrying variants of interest in case and control groups were tallied separately, and the p value was obtained from a one-tailed Fisher's exact test. In binomial pathway analysis, the observed number of rare damaging variants in LoF-intolerant genes that belong to statistically significant canonical pathways of interest were compared to the expected number of mutations in each set using a one-tailed binomial test. Gene sets of canonical pathways were obtained from IPA. The expected number of mutations in a given gene set is calculated as the formula below:

$$\text{Expected number of mutations} = N \times \frac{\sum_{Gene\ Set} \text{Gene Length}}{\sum_{Intolerant\ Genes} \text{Gene Length}}$$

Where N denotes total number of rare damaging *de novo* and transmitted mutations in intolerant genes as well as genes with significant burden of *de novo* and transmitted mutations.

Interactome Construction

We input all genes contributing to the significantly enriched pathway to String (version 10.5) (Szklarczyk et al., 2015). For organism, *Homo sapiens* was selected. For each displayed interaction, active interaction sources were restricted to experiments, and the maximum number of interactors was limited to 50.

In silico Modeling of Mutational Effects on Protein Structure

The sequence for all available modeled human proteins was downloaded from Uniprot (Apweiler et al., 2004). The stereochemical parameters of VOGM-associated mutations were analyzed using PROCHECK (Laskowski et al., 1993) and PROSA (Wiederstein and Sippl, 2007), and the final models were chosen based on the lowest energy function score (Dope) within the modeling program. The mutations were constructed and the free energy of change calculated ($\Delta\Delta G$) *in silico* using the ICM mutagenesis (Abagyan et al., 1994).

Cell Culture

HEK293T cells were passaged at 80%–90% confluence on high glucose DMEM (Dulbecco's modified Eagle's medium, GIBCO Life Technologies, Waltham MA, USA) supplemented with 10% fetal bovine serum (FBS, GIBCO Life Technologies Waltham MA, USA), L-glutamine, and penicillin/streptomycin.

Mutagenesis of Eph-B4 and Plasmid Transfection

A wild-type mouse *EPHB4* cDNA was sub-cloned into the pShuttle-IRES-hrGFP-2 plasmid vector with HA-Tag sequence (Protack et al., 2017). The QuikChange II Site-Directed Mutagenesis Kit (Aligent Technologies, Santa Clara CA, USA) was used to generate isolated single amino-acid changes within the *EPHB4* ORF (A509G, K650N, F867L). All mutant constructs were sequenced to confirm successful mutagenesis. The wild-type *EPHB4*, the mutant constructs, and empty vector were individually transiently transfected into HEK293T cells using Lipofectamine 2000 transfection reagent (Invitrogen, Carlsbad, CA, USA) according to its standard protocol. DNA complexes were removed after 5 h and replaced with fresh complete medium. After 48 hours, the medium was aspirated and the cells starved for 18 h in serum-free conditions.

Co-immunoprecipitation and Western Blotting

Cell lysates were prepared using NP40 lysis buffer (50 mM Tris, pH7.5; 1% Nonidet P-40; 150 mM NaCl; 10% Glycerol) containing protease and phosphatase inhibitor cocktail (Roche, Basel, Switzerland). Protein concentrations were measured with DC Protein Assay Reagents (Bio-Rad, Hercules CA, USA). For immunoprecipitation, equal amounts of cell lysates were incubated with Sepharose beads linked to anti-HA-Tag antibody (Cell Signaling Technology, Danvers, MA, USA) overnight at 4°C. Immunoprecipitated protein complexes were separated on SDS-PAGE gel and analyzed by western blotting using following antibodies: anti-phosphotyrosine P-Tyr-100, anti-HA-Tag, (Cell Signaling Technology, Danvers MA, USA), anti-Ras GAP (Santa Cruz Biotechnology, Dallas TX, USA). Band intensities were quantified using ImageJ software (Schneider et al., 2012). Statistical analyses were performed using Prism 7 software (GraphPad Software, La Jolla CA, USA).

DATA AND SOFTWARE AVAILABILITY

WES data for all VOGM parent-offspring trios reported in this study have been deposited in the NCBI database of Genotypes and Phenotypes (dbGaP). The accession number for the data reported in this paper is dbGaP: phs000744.v4.p2.